Journal of Materials Chemistry A

Opportunities for intermediate temperature renewable ammonia electrosynthesis

Journal:	*Journal of Materials Chemistry A*
Manuscript ID	TA-REV-04-2020-003753.R2
Article Type:	Review Article
Date Submitted by the Author:	22-Jul-2020
Complete List of Authors:	Fernandez, Carlos; Georgia Institute of Technology, George W. Woodruff School of Mechanical Engineering Hortance, Nicholas; Vanderbilt University, Interdisciplinary Department of Material Science Liu, Yu-Hsuan; Georgia Institute of Technology, School of Civil and Environmental Engineering Lim, JeongHoon; Georgia Institute of Technology, George W. Woodruff School of Mechanical Engineering Hatzell, Kelsey; Vanderbilt University, Mechanical Engineering; Vanderbilt University, Chemical and Biomolecular Engineering Hatzell, Marta; Georgia Institute of Technology, George W. Woodruff School of Mechanical Engineering

Journal Name

ARTICLE TYPE

Cite this: DOI: 00.0000/xxxxxxxxxx

Opportunities for intermediate temperature renewable ammonia electrosynthesis

Carlos A. Fernandez,*[a] Nicholas M. Hortance,[b]* Yu-Hsuan Liu[c], Jeonghoon Lim[a], Kelsey B. Hatzell[b] and Marta C. Hatzell[a]‡

Received Date
Accepted Date

DOI: 00.0000/xxxxxxxxxx

Production of ammonia using only renewable energy is achievable through various routes; however, direct electrochemical conversion technologies have achieved significant attention. Despite this attention, the promise for electrochemical ammonia synthesis is unclear, as most electrochemical technologies performance is well below that of the Haber-Bosch process (state of the art). Thus, there is a growing interest in defining realistic performance targets which would make renewable ammonia derived from electrochemical systems a reality. However, most efforts thus far have only explored optimizing single technology specific performance metrics such as faradaic efficiency. Optimization of this single performance metric often occurs at the expense of the rate of production which drives implementation and thus can be misleading. Here, we aim to outline the performance targets achievable for renewable ammonia produced through intermediate temperature electrosynthesis. Through exploring the thermodynamic and kinetic challenges, we will highlight the optimum expected rate of production and energy efficiency for intermediate temperature electrosynthesis. We also review current experimental reports focused on intermediate temperature ammonia electrosynthesis and detail materials related opportunities in catalyst and solid-electrolyte design. Finally, we discuss some of the challenges related to reporting these desired metrics due to measurement error, and offer solutions to mitigate these challenges.

1 Introduction

Mounting concerns regarding the carbon footprint of fertilizer production has stimulated growing interest in renewable ammonia. Renewable ammonia encompasses strategies to produce ammonia using non-fossil feedstocks in order to mitigate carbon emissions. These renewable approaches have centered primarily on low temperature (20-50 °C) and pressure (1-10 atm) technologies based around nitrogen electrocatalysis, photocatalysis, and plasma driven catalysis[1–4]. Electro- and photocatalysis are often deemed sustainable, as the only required reactants are air and water, and the only energy source is electricity or light. However, low temperature and pressure systems suffer from low rates of production (10^{-11} mol cm^{-2} s^{-1}), faradaic efficiency (10^{-2}-10 %), and energy efficiencies (1-2 %)[5]. Plasma-enable catalysis is a catalyst free approach which has exhibited high faradaic efficiency, but still suffers from low energy efficiency[4,6].

The low performance is unsurprising, as for a century, the Haber-Bosch process has only overcome these limitations through performing nitrogen reduction at elevated temperature (350-500 °C) and pressure (150-350 atm). The Haber-Bosch process achieves production rates which approach 6 g NH_3 kg_{cat}^{-1} min^{-1} at energy efficiencies of 60%[5,7]. This often equates to areal rates of production (i.e. rate normalized to the geometric area of the catalyst layer) similar to an electrocatalyst (10^{-11} mol cm^{-2} s^{-1}), yet the form factor of a catalyst bed reactor employed in thermocatalytic processes enable high volumetric catalyst loading since the catalyst does not need to be supported on an electrically conductive substrate (electrode).

In addition to electrocatalysis at ambient conditions, there has been numerous attempts to attain renewable ammonia through low pressure and high temperature routes. The three primary mid and high temperature routes include thermoelectrocatalysis, Haber-Bosch process with absorbent-based separations, and solar thermal ammonia production (STAP)[8–11]. All three approaches produce ammonia with energy efficiencies which approach that

[a] Georgia Institute of Technology, George W. Woodruff School of Mechanical Engineering, 771 Ferst Drive NW, Atlanta, Georgia, USA. E-mail: marta.hatzell@me.gatech.edu
[b] Vanderbilt University, Interdisciplinary Material Science,2301 Vanderbilt Place, Nashville, Tennessee, USA.
[c] Georgia Institute of Technology, School of Civil and Environmental Engineering, 790 Atlantic Dr, Atlanta, Georgia, USA. E-mail: marta.hatzell@me.gatech.edu

† Electronic Supplementary Information (ESI) available: See DOI: 00.0000/00000000.

* Authors N. M. Hortance and C. A. Fernandez contributed equally to this work.

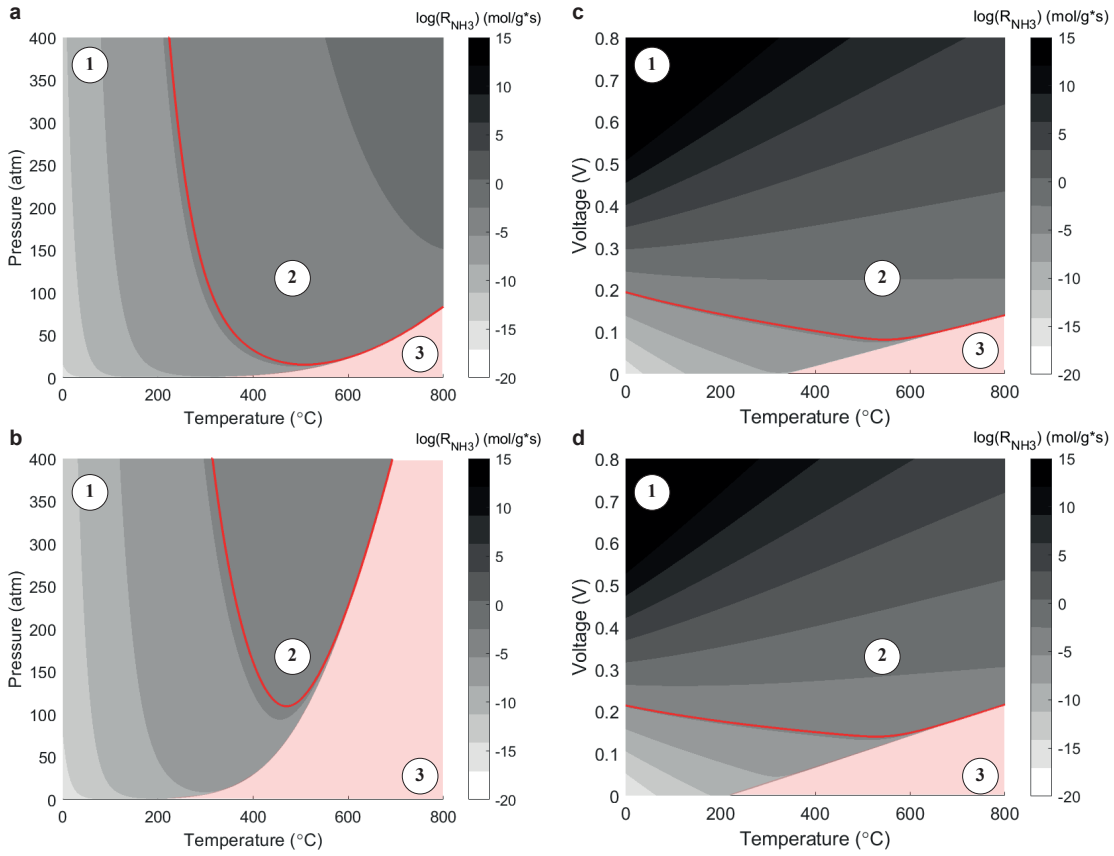

Fig. 1 Ammonia production rate for thermochemical synthesis with an ammonia molar fraction of 1% (a) and 10% (b), and for electrochemical synthesis at ambient pressure with an ammonia molar fraction of 1% (c) and 10% (d). The red line indicates the conditions necessary to obtain a similar rate to the Haber-Bosch process. The red region highlights where the thermodynamic equilibrium prevents the production of ammonia. The figure has three regions (1,2, and 3) representing the three temperature regimes (low $\leq$300 °C , intermediate 300-600 °C, and high >600 °C). A detailed explanation of the analysis used to develop this figure can be found in the supplementary information.

achieved through large-scale Haber-Bosch process (60%).[5] Despite these promising routes, low pressure-high temperature systems are often under investigated, because of an increasing emphasis on ambient temperature processes.

The range of approaches to attain renewable ammonia prompt a need to better understand the thermodynamic and kinetic limitations of each approach. Herein, we discuss the relevant theoretical and experimental motivations for electrochemical synthesis of ammonia at intermediate temperatures and low pressure. We also discuss the potential materials related challenges which need to be addressed for intermediate ammonia synthesis to come to fruition. Lastly, we highlight challenges with ammonia detection, and suggests approaches for overcome this limitation.

2 Performance Considerations for Intermediate Temperature Ammonia Electrosynthesis

Electrochemical systems are attractive alternatives to the Haber-Bosch process because they enable the transformation of electrical energy into chemical energy, using primarily an applied voltage as the driving force for catalysis. In theory, an electrochemical reactor can achieve nitrogen conversions which approach those attained through the Haber-Bosch process[12]. Yet, thermodynamics are not the only considerations for determining whether a catalytic process is effective. Ultimately, the rate of ammonia production is also essential for determining if a technology is economically and technically useful. This requires a thorough understanding of the kinetics of the reaction under standard operating conditions.

2.1 Kinetic Considerations

A thermochemical reactor operating at low temperature results in low production rates at nearly all pressures (Fig. 1a,b – zone 1). Increasing the temperature only marginally increases production rates, as the shifting equilibrium point begins to favor ammonia decomposition. Thus, a reactor operating at high temperature suffers from low conversion efficiency (Fig. 1a,b – zone 3). The use of elevated pressure is necessary to offset this equilibrium shift, and maximize product yield in the Haber-Bosch process. The optimal operating temperature and pressure for thermocatalytic conversion of nitrogen to ammonia also depends on the concentration of ammonia in the reactor. For instance increasing the concentration from 1% (Fig. 1a) to 10%(Fig. 1b) shifts the optimum temperature and pressure. Overall, optimal operation occurs at intermediate temperature ($\sim$400 °C) and moderate pressure ($\sim$ 200 atm)(Fig. 1a,b – zone 2).

In an electrocatalytic reactor, an applied voltage drives the cat-

alytic process instead of temperature (Fig. 1c and d). Theoretically, an electrochemical cell can achieve similar production rates as a thermocatalytic reactor. For instance, if the cell voltage is increased to 210 mV, an electrochemical reactor can achieve a production rate comparable to a thermocatalytic reactor at ambient temperature (red line represents a production rate of 6x10^{-6} mol g^{-1} s^{-1}). This cell voltage is equivalent to a 260 mV overpotential. However, this high overpotential is often deemed prohibitively expensive because the cost of electricity dominates the cost of the product (levelized cost of ammonia – LCOA) [13,14]. To put this overpotential into perspective, in water electrolysis (hydrogen production), the hydrogen evolution reaction overpotential is only on the order of 10-100 mV [15]. We will also note that the reaction overpotential may be even larger in practice, as the kinetic model must make assumptions regarding kinetic constants (See Supporting Information).

Thus, in order for electrochemical ammonia synthesis to become viable, efforts are needed to reduce the the nitrogen reduction reaction overpotential, to reduce the LCOA. There are significant bottom-up efforts on-going in the area of catalyst design which aim to reduce catalyst surface overpotential. However, these approaches have yet to discover or identify any effective highly active catalyst for nitrogen reduction at ambient conditions. Thus, alternative system operations-based strategies should also be explored to enhance the rate of production. One immediate way to reduce the required overpotential is to alter the system operating temperature (Fig. 1c,d). Increasing the temperature of the cell the intermediate range ($<$ 600 °C), can reduce required cell voltage by 33% ($\sim$ 140 mV) and eliminate the activation overpotential ($\sim$ 1 mV), (Fig.1c,d – zone 2). This is still energy intensive, but is a better entry point for electrochemical ammonia synthesis. Operation at high temperature ($>$ 600^{o}C) still results in ammonia decomposition, and thus is not advisable (Fig. 1c,d – zone 3). An additional advantage of an electrochemical system over a thermocatalytic systems is the ability to attain a desired production rate over a wider range of temperature and concentration (ammonia). In thermochemical systems, the required pressure to maintain the same production rate increases by 300% when the concentration of ammonia increases from 1% to 10% for a thermochemical reactor operating at 400^{o}C. A similar increase in ammonia concentration only requires a 75% increase in the required voltage for an electrochemical reactor operating at 600^{o}C.

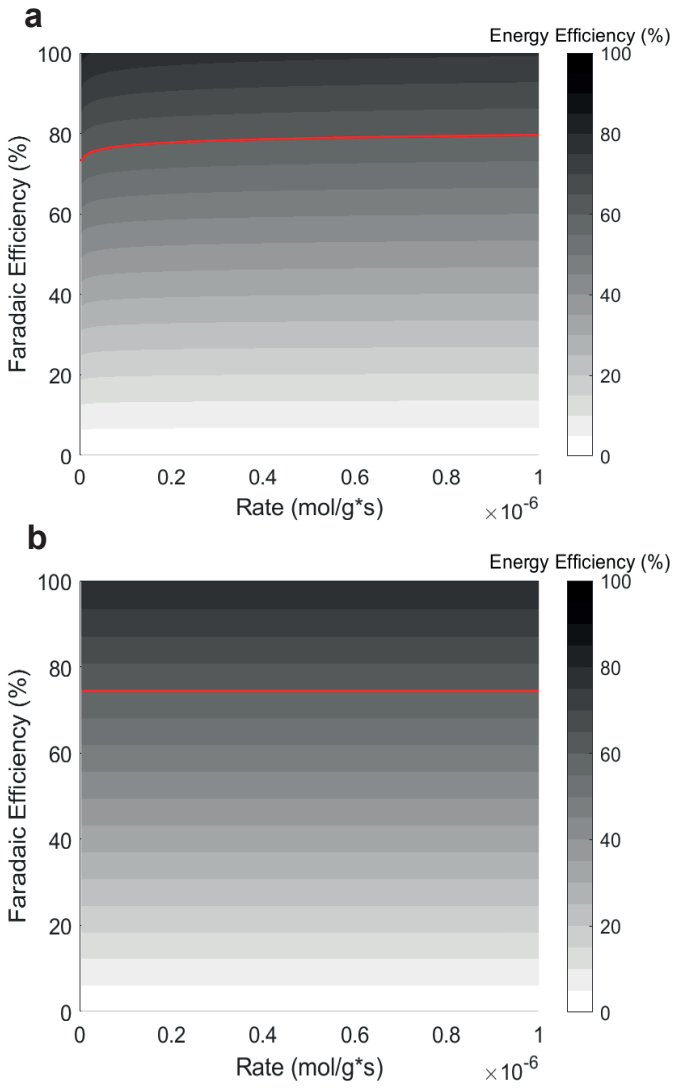

Fig. 2 Energy efficiency of a low temperature electrochemical ammonia synthesis cell (25^{o}C), with a reference exchange current density of 10^{-10} A cm^{-2}, an electrolyte ionic conductivity of 0.1 S cm^{-1} (Nafion), a electrolyte thickness of 60 μm, and catalyst loading is 1 mg cm^{-2}(a). Energy efficiency of a intermediate temperature electrochemical ammonia synthesis cell (600^{o}C), with a reference exchange current density of 10^{-10} A cm^{-2}, an electrolyte ionic conductivity of 0.014 S cm^{-1}, a electrolyte thickness of 50 μm, and catalyst loading is 1 mg cm^{-2}(b) Red line indicates an achievable energy efficiency for the Haber-Bosch process.

2.2 Energy Efficiency Considerations

The Haber-Bosch process is highly efficient (60%) [5] when compared to electrochemical synthesis-based technologies (1%) [5]. Improving the Haber-Bosch energy efficiency further is possible (thermodynamic limit is $\sim$ 90%) [16], and efforts which succeed in increasing this efficiency will aid in minimizing the carbon emissions associated with the Haber-Bosch process. However, energy efficiency improvements are not necessary to promote the economic viability of the Haber-Bosch process. Conversely, energy efficiency improvements are imperative in order to improve the economic viability of electrochemical ammonia synthesis system. This is due to the innate connection between energy efficiency and system size (capitol cost), and energy usage (operating costs).

The energy efficiency for an electrochemical system is largely governed by the system faradaic efficiency. A faradaic efficiency of 100% indicates that all the current is utilized to reduce nitrogen, and a faradaic efficiency of 0% indicates that no current is utilized to reduce nitrogen. In the case where faradaic efficiency is negligible, the electrons most likely are used to produce hydrogen, an unwanted side product. Most nitrogen reduction electrocatalysts today achieve faradaic efficiencies between (10^{-2}-10%) [5]. Higher faradaic efficiencies have been reported, but typically are

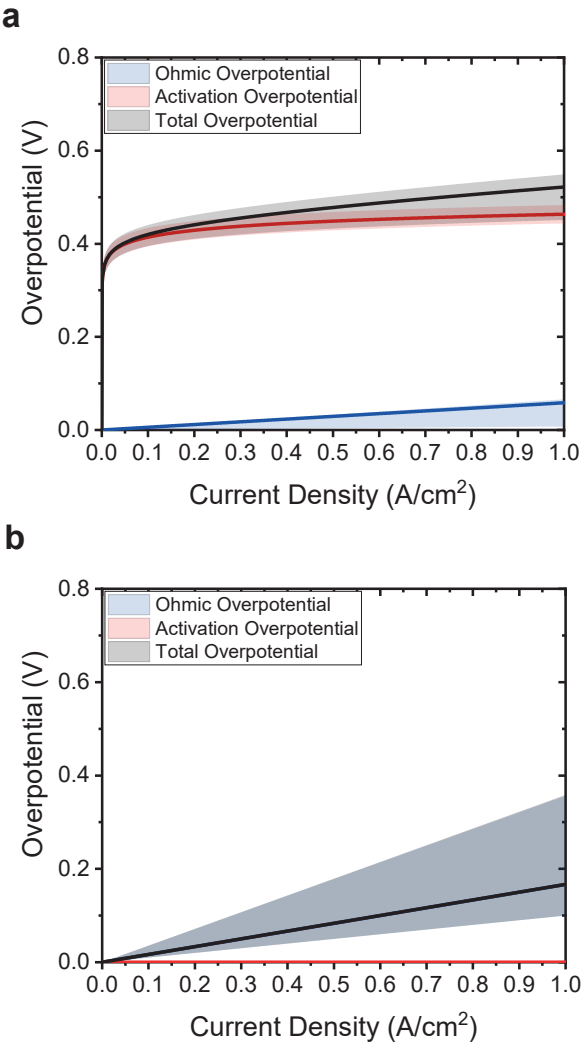

Fig. 3 Projected cell overpotentials for a low temperature ammonia electrosynthesis reactor (25^{o}C) (a), and intermediate temperature ammonia electrosynthesis reactor (600^{o}C) (b).

obtained at impractically low current[5].

Increasing faradaic efficiency requires the design of catalyst with a high degree of selectivity for nitrogen reduction. This is a significant challenge as the redox potential for nitrogen reduction (E°=0.056 vs RHE at 25°C and E°=-0.140 vs RHE at 600°C) resides close to the more facile hydrogen evolution reaction (E°=0 vs RHE). Furthermore, most surfaces preferentially bind H* rather than N* which promotes the formation of few active sites for nitrogen activation. Catalyst design and system operations are therefore critical in order to overcome these challenges (see sec. 3.2).

In order for low-temperature electrochemical ammonia synthesis to approach the energy efficiency of the Haber-Bosch process (∼60%), the system needs to approach ∼80% (Fig. 2a). This is not feasible with aqueous-based electrolytes, and is even challenging in a non-aqueous environment at relevant current densities. The required faradaic efficiency for an intermediate-temperature electrochemical ammonia synthesis system to approach the energy efficiency of the Haber-Bosch process is 75% (Fig. 2b). This is still ambitious. To put this into perspective, carbon dioxide based electrolysis systems, have been able to obtain faradaic efficiency which approach 50-80% for the conversion of CO_2 to CO[17,18]. Even though the electrical energy required by an intermediate-temperature system is lower than the electrical energy required by a low-temperature system, the total energy required is equivalent in both systems due to the additional heat input in intermediate-temperature system to increase the temperature of the reactants. This suggests that both low and intermediate temperature electrolysis cells may not be able to achieve energy efficiencies which meet the Haber-Bosch process. Therefore, practical targets for energy efficiency are necessary. As with all renewable technologies, the energy conversion efficiencies targets will not need to approach that of thermal systems. This is because of the relative abundance of renewable energy (sun) when compared to fossil fuels. However, in order to limit system size energy efficiencies on the order or 20-40% may be ideal.

Increasing the energy efficiency of the system can also be accomplished through reducing system losses. While a complete electrochemical systems will have many components (compressors, pumps, separation devices), most system losses are associated with the electrochemical cell. Losses within the electrochemical cells, termed overpotentials, must be reduced to maximize efficiency. The three primary overpotentials are ohmic, activation, and mass transport losses.

The largest ohmic loss in an electrochemical reactor is due to the ionic conductivity of the electrolyte. Within low temperature electrolysis systems, the electrolyte is largely polymer based, and the conductivity (inverse of resistance) increases moderately with temperature (Fig. S3)[19,20]. The low temperature electrolytes have conductivity order of 0.1 S cm^{-1} [19] (Fig. 3a). For intermediate temperature operation, the ionic conductivity of solid electrolytes is highly dependent on temperature. Solid electrolytes have poor ionic conductivity at low temperatures (0.002 S cm^{-1})[20], but improve at intermediate and high temperatures (0.01-0.04 S cm^{-1} – Table 1). Therefore, even when operating optimally the intermediate temperature solid electrolytes are about an order of magnitude more resistive than the low temperature polymer based electrolytes (Fig. 3b). For this reason, the ohmic losses are generally negligible with respect to the other losses in a low temperature electrolysis cell, but dominant cell losses in a intermediate temperature electrolysis cell(Fig. 3).

The activation overpotential depends on the kinetics of the reaction, and improves as temperature increases due to the Arrhenius relationship. A reactor operating at ambient temperature has an activation overpotential of 400 mV. As temperature increases to 600°C, the activation overpotential decreases to as low as 0.3 mV. For these reasons, highly active electrocatalyst (such as certain precious metals) are desirable for low temperature cells, whereas less active (such as earth abundant metals) electrocatalyst are generally acceptable for higher temperature cells. Temperature effects will have a marginal impact on transport related losses. Increasing the temperature increases the diffusivity of nitrogen in aqueous media, allowing for a slight decrease in mass

transport losses. Higher temperatures will also promote the use of gas-diffusion layer based cells which have significantly less transport related losses than liquid aqueous phase systems[21].

As ammonia electrosynthesis continues to grow, care must be placed on understanding each system level limitation. Catalyst design is highly important for achieving high faradaic efficiency. However, in order to approach the reaction rates and energy efficiency of the Haber-Bosch process, higher temperature operations should be investigated. In the subsequent section, we summarize the current state-of-the-art in electrolyte and catalyst materials.

3 Current Progress in Intermediate Temperature Ammonia Electrosynthesis

The central component of a solid oxide electrolysis cell is the membrane electrode assembly, which is composed of two electrodes (anode and cathode) and a dense solid electrolyte. When a proton conducting electrolyte is employed, N_2 reduction and H_2/H_2O oxidation reactions occur separately at the cathode and anode (Fig. 4a). In contrast, N_2 reduction and H_2O dissociation occur at a single electrode (cathode) in the electrolysis cell with an oxygen ion-conducting electrolyte. Thus, oxygen ion-conducting electrolytes are challenging to implement and are fundamentally limited by the cathode electrocatalyst (detailed in Section 3.2).

All components must exhibit chemical and mechanical stability at intermediate temperatures (200-650°C) to be viable for electrosynthesis. The anode and cathode electrodes are ideally porous to enable gas transport and are comprised of an inorganic mixed ion and electron conductor and an active catalyst (Fig. 4). The solid electrolyte must show high ionic conductivity, chemical compatibility with the catalyst, and negligible electronic conductivity. Trace electronic conductivity in a solid electrolyte can decrease the transference number and current efficiency of a cell. Thus, material interactions between the catalyst, electrode, and electrolyte is immensely important for engineering durable solid oxide electrolysis cells.

This section aims to highlight the current state-of-the-art materials for ammonia electrosynthesis. In particular, we discuss how materials can be engineered to enhance the rate of production and energy efficiency of the electrochemical cell. Specific attention is focused on identifying pathways toward achieving high faradaic efficiencies (>70%) and high ionic conductivities (>0.1 S cm^{-1}). A full review of these materials can be found elsewhere[22–24].

3.1 Solid Electrolytes

The most common solid electrolytes used are proton, oxide ion, and nitride ion conductors. With the exception of oxygen conductors, the ions being conducted through the electrolyte may also serve as hydrogen or nitrogen sources for ammonia synthesis. Often, the solid electrolytes are made from ceramic based materials, and thus conductivity is heavily dependent on temperature (200 - 650°*C*). Below we briefly discuss opportunities for solid electrolyte design.

3.1.1 Proton Conducting Inorganic Electrolytes

Inorganic proton solid electrolytes are the most common electrolyte. There are three families of proton conducting electrolytes being explored for intermediate temperature ammonia electrosynthesis: (1) solid acids[25–28], (2) oxides (perovskites, flourites, pyrochlores) (Fig.5)[22,29–32], and (3) composite electrolytes (oxide/binary phosphates and oxide/ternary carbonates).

Solid acid electrolytes were first introduced in 2001 and operate between 100-300°C[33]. Common stoichiometries for solid acid electrolytes are $MHXO_4$, MH_2XO_4, and $M_3H(XO_4)_2$, where *M* can be Cs, Rb, K, Na, and/or NH_4, and *X* can be P, S, Se, and As. Fundamentally, this family of electrolytes are comprised of oxyanions (e.g. SO_4^{2-}, SeO_4^{2-}, etc.) that are connected together via hydrogen bonds[26,34]. As the operating temperature increases from 100 to 300°C a phase transition occurs which results in a more disordered structure, and subsequently an order of magnitude increase in the ionic conductivity. This increase in ionic conductivity is associated with rapid reorientation of XO_4^{2-} anion groups which enables more facile proton transport between neighboring anion groups[26,34].

One of the most promising solid acid electrolytes is CsH_2PO_4. This electrolyte transforms from a monoclinic to a cubic phase upon heating at ≈228°C and experiences a four-fold increase in the ionic conductivity (>10^{-2} S cm^{-1})[35]. The melting temperature of a solid acid electrolyte can vary widely depending on the stoichiometry. One strategy employed to increase the melting temperature is the introduction of oxide (e.g. SiO_2) or pyrophosphate (SiP_2O_7)[36,37]. CsH_2PO_4/SiP_2O_7 composites form $CsH_5(PO_4)_2$ at the interfaces of the two materials which leads to higher ionic conductivities at lower temperatures. Furthermore, this composite demonstrates a nearly constant ionic conductivity ($\geq$ 20 mS cm^{-1}) between 100 to 270°*C*[37,38] (Fig. 6). Finally, the addition of SiP_2O_7 reduces the solid electrolyte's plasticity which enables more compliant interfaces and less short-circuiting.[35]

Recently, a wide-range of solid acid electrolytes (e.g. $CsHSO_4$[39]; $Rb_3H(SeO_4)_2$[40]; and $(NH_4)_3H(SO_4)_2$[41]) have been explored for electrosynthesis of ammonia. A significant challenge

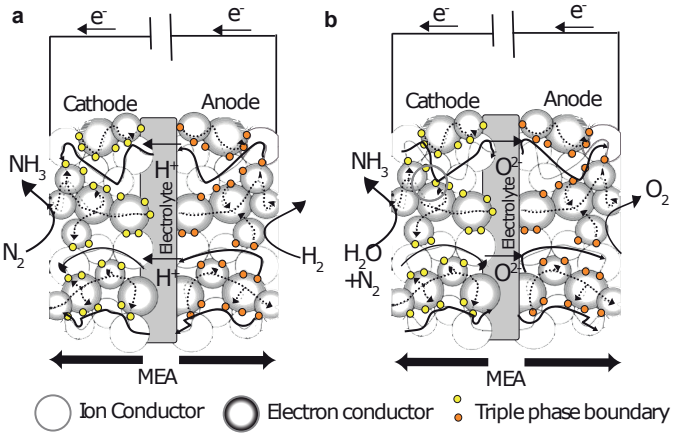

Fig. 4 (a) Proton and (b) oxygen-ion conducting solid electrolytes have been investigated for intermediate temperature ammonia electrosynthesis cells.

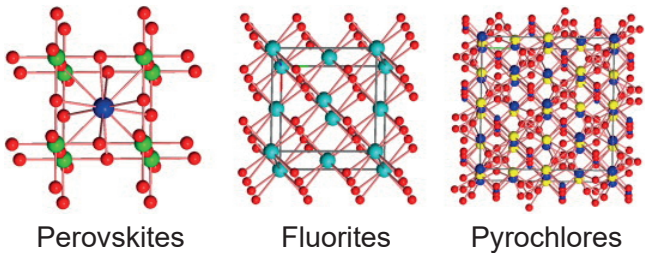

Fig. 5 The primary solid electrolytes investigated for intermediate electrosynthesis of ammonia are perovskites, fluorites and pyrochlores (Reproduced with permission [22], Elsevier).

with solid acid electrolytes is electrolyte decomposition when in contact with a base (e.g. NH_3). One solution explored in the literature is the use of a proton conducting barrier film (e.g. AgPd), coated directly onto a CsH_2PO_4/SiP_2O_7 solid electrolyte. The barrier film mitigates acid/base interactions, enables proton transport, and allows for the use of dry gases (e.g. H_2) [42,43]. A faradaic efficiency around 2.6% was achieved using a barrier film. Another study examined a barrier-free CsH_2PO_4/SiP_2O_7 electrolyte with a range of noble-metal catalysts and could only achieve faradaic efficiencies ~0.15%. In the absence of a barrier, it is necessary to utilize humidified gases to avoid dehydration [38]. Overall, the faradaic efficiency and synthesis rate were shown to decrease at voltages greater than 0.3V. At low voltages (0.15V) all catalysts (except Ru) showed similar synthesis rates of $0.8*10^{-10}$ mol $cm^{-2}*s$ at 220°C [38]. A wide range of side reactions can occur at elevated voltages including (1) the electrolyte decomposition at the catalyst|electrolyte interface and (2) the formation of hydrogen gas. Thus, low electrosynthesis voltages are desirable to avoid side reaction and achieve high energy efficiency in solid acid electrolytes.

The second family of electrolytes being explored for intermediate temperature ammonia electrosynthesis are oxide solid electrolytes. Three prominent proton conducting oxides include: (1) perovskite, (2) flourite, and (3) pyrochlore (Fig. 5). Proton transport in oxides primarily occurs through the Grotthuss mechanism which involves proton hopping between neighboring oxygen atoms [51,52]. Transport properties can be tuned via increasing the concentration of protonic defects (e.g. OH^- or oxyanions) [53]. Tuning the defect chemistry via elemental doping is one strategy often employed to increase the oxygen vacancy concentration [26,34]. These solid electrolytes typically operate between 400 and 650°C. Thus, the operating temperature is similar to the Haber-Bosch and can even exceed it at times. Thermodynamically, ammonia decomposition at these temperatures is possible as discussed in Section 2, and should be avoided.

The ion in the electrolyte can act both as a charge carrying element and as a catalytic promoter. The mobile ion in the electrolyte can dynamically alter the electronic structure of the catalyst and influence the binding energies of the reactant and/or adsorbed molecules [54–56]. This phenomena is known as non-Faradaic electrochemical modification of catalytic activitiy (NEMCA) [57,58] or electrochemical promotion of catalysis (EPOC) [59,60]. Thus, control over transport within the electrolyte

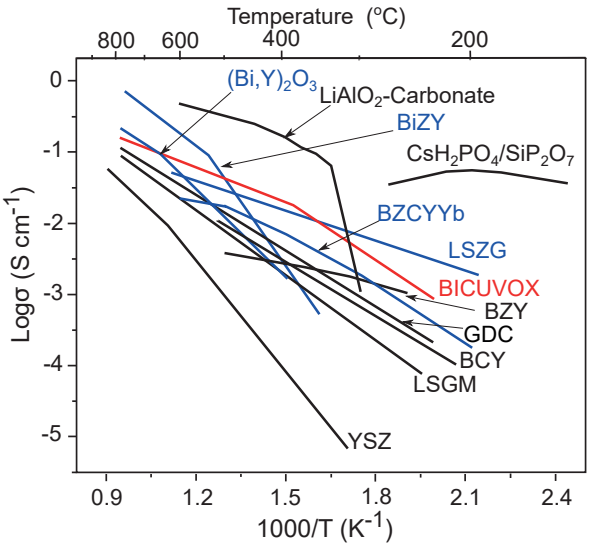

Fig. 6 Ionic conductivity of common electrolytes (O^{2-} and H^+ conductors) that have or have not yet been used for ammonia synthesis; $(Bi,Y)_2O_3$, $LiAlO_2$-Carbonate [44]: $LiAlO_2$-$(Li,Na,K)_2CO_3$, BZY: $BaZr_{0.8}Y_{0.2}$, LSZG [45]: $Li_{13.9}Sr_{0.1}Zn(GeO_4)_4$, BICUVOX [46]:$Bi_2V_{1.9}Cu_{0.1}O_{5.35}$, BZCYYb [47]:$BaZr_{0.4}Ce_{0.4}Y_{0.1}Yb_{0.1}$, GDC [48]:$Ce_{0.9}Gd_{0.1}O_{1.95}$, LSGM [46]: $La_{0.9}Sr_{0.1}Ga_{0.8}Mg_{0.2}O_{2.85}$, YSZ [49]: 8%$Y_2O_3/ZrO_2$, BCY [50]:$BaCeO_3$ $Cs_2H_2PO_4/SiP_2O_7$ [38]. Blue: H^+ conducting electrolytes not yet used for ammonia synthesis; Red: O^{2-} conducting electrolytes not yet used for ammonia synthesis; Black: Electrolytes previously used for ammonia synthesis

and at the electrolyte|electrode interface may provide a pathway toward controlling adsorbates and reaction kinetics.

Perovskite's have the general form ABO_3, where A is typically Ba, Sr, Ca and/or La and B is either Ce or Zr. Oxygen vacancies in perovskite oxides determine material structures and properties such as ionic charge transport. The concentration of oxygen vacancies can be increased via doping the B-site with aliovalent cations such as yttrium or ytterbium. Perovskites with cerium ions in the B-site demonstrate a high ionic conductivity due to its exceedingly negative hydration enthalpy (e.g. -162.2 kJ/mol for $Ba(Ce_{0.9}Y_{0.1})O_{3-\delta}$ [61]). Hydroxyl terminating groups can be retained at high temperatures when the hydration enthalpy becomes increasingly negative [62]. However many bulk electrolytes that have cerium atoms in the lattice are chemically unstable due to the formation of carbonates (e.g. as in the case of $BaCeO_3$ and $SrCeO_3$) [26,53]. Thus, zirconium and yttrium are doped into the B-site of these cerates to promote stability. [30]

Early work using a perovskite, proton-conducting strontia-ceria-ytterbia (SCY) electrolyte ($SrCe_{0.95}Yb_{0.95}O_3$), explored ammonia decomposition during ammonia synthesis at elevated temperatures (≥500°C) [58]. At 750°C, using symmetric Pd electrodes, a synthesis rate ~$4.8*10^{-9}$ mol $cm^{-2}s^{-1}$ was achieved. Furthermore, ammonia decomposition was shown to decrease at these high temperatures due to the NEMCA effect. In particular, proton 'spillover' can spread on the metal catalyst and form dipoles which decreases the catalyst potential. In this particular work, this led to a decrease in the catalyst's binding strength to electron donating adsorbates such as NH_3 [58,63]. The latter effect is attributed

to the decrease in ammonia decomposition. In a follow up study, contrary results were observed for a SCY electrolyte coupled with Ag catalysts. This system experienced increases in ammonia decomposition upon applying a constant current[64]. These results suggest that the nature of the triple boundary and local electric field may play a role on the local binding energy. Additional investigations have been conducted using an SCY electrolyte with catalysts (e.g. Ag, AgPd) with little improvement to the synthesis rate[31,64,65]. Low synthesis rates have been attributed to low ionic conductivity and high ohmic resistances in SCY(Fig. 6).

Alternatively, there has been a significant interest in highly conducting $BaCeO_3$-based and $BaZrO_3$-based perovskite solid electrolytes. To improve the ionic conductivity the *B*-site is doped with yttrium to produce the commonly known BCY and BZY solid electrolytes. $BaCe_{0.85}Y_{0.15}O_{3-\delta}$ (BCY) was implemented in a symmetric AgPd cell and obtained ammonia at a rate of 2.1×10^{-9} mol $cm^{-2}s^{-1}$ and efficiency above 60% at 500°*C* in a humidified hydrogen environment.[66] The electrolyte's transference number for protons (i.e fraction of current for protons relative to the total current) was near unity, but began to decrease as the applied current exceeded 12 mA cm^{-2}. This phenomenon was attributed to polarization of the electrode and a reduced concentration of protons at the interface between the electrolyte and electrocatalyst. This however did not affect the synthesis rate since the optimal current density was found to be 0.75 mA cm^{-2}. Barium cerates (e.g. BCY) are chemically unstable with acidic reactants, while barium zirconates are known to be more stable. Table 1 summarizing the performances properties for a range of BZY and BCY electrolytes tested for electrosynthesis of ammonia.

Fluorite (AO_2) and pyrochlore ($A_2B_2O_7$) structured proton conductors are also used for ammonia electrosynthesis (Table 1). Fluorite structured electrolytes have oxygen ions in cubic packing and tetravalent metal cations in alternating cube centers (Figure 5). Pyrochlores have an ordered defective fluorite structure where the *A* and *B* atoms are trivalent and tetravalent cations, respectively. Previously a $AgPd|La_{1.9}Ca_{0.1}Zr_2O_{6.95}|AgPd$ cell synthesized ammonia at a rate of 2×10^{-9} mol $cm^{-2}s^{-1}$ and had a faradaic efficiency of 80% at 500°*C* using hydrogen and nitrogen.[67] Calcium doping causes the grains to enlarge and increases the grains and the grain boundary ionic conductivity.

The final type of proton conducting solid electrolyte being studied in ammonia electrosynthesis are composite electrolytes. These electrolytes combine two different types of ion conducting media and may actually have multiple charge carriers (i.e. H^+ and N^{3-}): (1) oxide and (2) phosphates or carbonates[44,68–70]. Combining multiple ion conductors together can enable tunable material properties (e.g. transport, thermal, mechanical, and/or electrical) (Fig. 6). Ternary, carbonate-based composite electrolytes commonly use $(Li,Na,K)_2CO_3$ because it has a relatively low melting point (396°*C*) and can achieve ionic reasonable ion conductivities (100 mS cm^{-1}) at 400°*C*[71]. Recently, a ceria-$Ca_3(PO_4)_2$-K_3PO_4 electrolyte was used to synthesize ammonia, where the hydrogen source was natural gas[68,69]. A synthesis rate ~6.95*10^{-9} mol $cm^{-2}s^{-1}$ was achieved at 650°C. Interestingly, this electrolyte saw increases in ammonia synthesis rate as the temperature increased from 400 to 650°C, suggesting that ammonia decomposition was not affected by the temperature increase. However, in another study using a $LiAlO_2$-carbonate electrolyte with a AgPd anode and a Fe_3Mo_3N-Ag cathode synthesized ammonia at a rate of 1.88×10^{-10} mol $cm^{-2}s^{-1}$ with a Faradaic efficiency of 1.84% at 425°*C*. In this study the rate and efficiency decreased as the temperature increased, suggesting ammonia decomposition played a role. Thus, the nature of ammonia decomposition in these mixed material systems are not well understood. Composites may be a pathway forward to tailor interfaces for either chemical stability or directed transport. Table 1 summarizes the current performance results for all reported composite electrolytes.

3.1.2 Proton Conducting Polymer Electrolytes

Proton conducting polymer electrolytes such as perfluorosulfonic acid (e.g. Nafion) are typically used in ambient, low temperature electrosynthesis. However, Nafion operationally is limited to $\leq 90°C$;[104,105] and recent studies suggest that they may not be suitable because it has a tendency to absorb ammonia resulting in accelerated decomposition of Nafion.[106] Despite the lack of studies, intermediate temperature synthesis of ammonia could benefit from using polymer electrolytes. High-temperature, polymer electrolyte membranes (HT-PEMs) are capable of operating within 100 to 200°*C* without the need of humidification (as is the case for Nafion). Phosphoric acid doped polybenzimidazole (PBI) is a well-known high temperature membrane investigated for its use in H_2/O_2 fuel cells, wherein it attains a power density within 500 - 800 mW/cm^2 at 100 to 200°*C* in a hydrogen/air mixture.[107] By comparison, solid oxide fuel cells attain power densities near 100 mW cm^{-2} at 350°*C* and 1400 mW cm^{-2} at 700°*C*[108,109]. However, steam cannot be used as a hydrogen source with PBI electrolytes because it will cause a loss in phosphoric acid groups. A more promising polymer is the SnP_2O_7/Nafion composite, which attains a high ionic conductivity of 100 mS cm^{-1} at 200°*C*, a similar power density of 800 mW cm^{-2}, and is stable in dry and wet conditions for over 1400 hours.[110] Polymer electrolytes that can sustain higher temperatures represent a very promising area for growth because scalable manufacturing methods are available. However to date there have been limited investigations that have been reported.

3.1.3 Oxygen Conducting Ceramic Electrolytes

An alternative to proton conducting electrolytes are oxide ion conducting electrolytes. The charge carrier (i.e. oxide ion) does not react in either the anode or cathode half cell reactions. Instead, steam and nitrogen are reactants at the cathode and are reduced to form ammonia. The two half-cell reactions that occur in a fuel cell configuration, operating with an oxide conducting electrolyte are (Fig. 4b):

$$3H_2O + N_2 + 6e^- \longrightarrow 3O^{2-} + 2NH_3$$
$$3O^{2-} \longrightarrow \tfrac{3}{2}O_2 + 6e^-$$

Yttrium stabilized zirconia (YSZ), is a common oxide-conducting electrolyte comprised of $8\%Y_2O_3/ZrO_2$. Previously, a double-chamber set-up with a Ag|YSZ|Ru-Pd cell, demonstrated a synthesis rate of $1.5*10^{-13}$ mol $cm^{-2}s^{-1}$ at 650°*C*, with steam and nitrogen reactants.[72] The synthesis rate increased to nearly $7.5*10^{-13}$

Table 1 Intermediate temperature ammonia electrosynthesis performance

Electrolyte	$H^+/O^{2-}/N^{3-}$	Catalyst	Rate (mol×cm^{-2}s^{-1})	Temperature (^{o}C)	Conductivity (mS cm^{-1})	Ref
8% Y_2O_3/Zr_2O_3	O^{2-}	Pd-Ru/MgO(C), Pd(A)	1.5×10^{-13}	650	X	72
$Ce_{0.9}Gd_{0.1}O_{2-\delta}$	O^{2-}	Pt(C&A)	3.67×10^{-11}	600	X	73
$Ce_{0.8}La_{0.2}O_{2-\delta}$	H^+/O^{2-}	AgPd(C&A)	7.2×10^{-9}	650	19 @ 650^{o}C	74
$Ce_{0.8}Y_{0.2}O_{2-\delta}$	H^+/O^{2-}	AgPd(C&A)	7.5×10^{-9}	650	23 @ 650^{o}C	74
$Ce_{0.8}Gd_{0.2}O_{2-\delta}$	H^+/O^{2-}	AgPd(C&A)	7.7×10^{-9}	650	26 @ 650^{o}C	74
$Ce_{0.8}Sm_{0.2}O_{2-\delta}$	H^+/O^{2-}	AgPd(C&A)	8.2×10^{-9}	650	38 @ 650^{o}C	74
$SrCe_{0.95}Yb_{0.05}O_{3-\delta}$	H^+	Ag-Ru/MgO(C), Pd(A)	3×10^{-13}	650	X	72
$SrCe_{0.95}Yb_{0.05}O_{3-\delta}$	H^+	Pd (C&A)	6.5×10^{-12}	570	X	63
$SrZr_{0.95}Y_{0.05}O_{3-\delta}$	H^+	Fe (C) Ag (A)	2.2×10^{-9}	450	X	75
$BaCe_{1-x}Y_{0.15}O_{3-\delta}$	H^+	AgPd (C&A)	2.1×10^{-9}	500	X	66
$BaCe_{0.7}Zr_{0.2}Sm_{.10}O_{3-\delta}$	H^+	AgPd (C&A)	2.67×10^{-9}	500	X	76
$BaCe_{1-x}Y_{0.2}O_{3-\delta}$	H^+	AgPd (C&A)	2.36×10^{-9}	500	X	77
$BaCe_{0.5}Zr_{0.3}Y_{0.16}Zn_{0.04}O_{3-\delta}$	H^+	Fe/Pd(C),NiO&CeO_2(A)	4×10^{-9}	450	X	78
$BaZr_{0.7}Ce_{0.2}Y_{0.1}O_{2.9}$	H^+	Ni(C), Cu(A)	4.1×10^{-9}	620	X	79
$BaCe_{0.65}Zr_{0.2}Er_{0.15}O_{3-\delta}$	H^+	Pt(C&A)	3.27×10^{-9}	450	1.0 @ 600^{o}C	80
$BaCe_{0.85}Gd_{0.15}O_{3-\delta}$	H^+	Ag-Pd(C),Ni-BCGO(A)	4.63×10^{-9}	480	14 @ 600^{o}C	20
$BaCe_{0.85}Y_{0.15}O_{3-\delta}$	H^+	Ag-Pd(C),Ni-BCY(A)	4.1×10^{-9}	530	3.0 @ 600^{o}C	81
$La_{1.9}Ca_{0.1}Zr_2O_{6.95}$	H^+	AgPd (C&A)	1.76×10^{-9}	520	X	82
$BaZr_{0.8}Y_{0.2}O_{3-\delta}$	H^+	Ag(C&A)	4.9×10^{-11}	550	2.0 @ 600^{o}C	83
$BaZr_{0.8}Ce_{0.1}Y_{0.1}O_{3-\delta}$	H^+	VN(C),Ni-BCY72(A)	1.9×10^{-9}	600	X	84
$BaCe_{0.7}Zr_{0.1}Gd_{0.2}O_{3-\delta}$	H^+	Ni-BCZG(C&A)	1.87×10^{-10}	500	19 @ 600^{o}C	85
$BaCe_{0.9}Y_{0.1}O_{3-\delta}$	H^+	Fe-BCY(C),Pt(A)	6.7×10^{-10}	650	X	86
$BaCe_{0.9}Y_{0.1}O_{3-\delta}$	H^+	Ni-BCY(C&A)	3.36×10^{-10}	500	X	87
$BaCe_{0.9}Y_{0.1}O_{3-\delta}$	H^+	Ni-BCYR(C),Ni-BCY(A)	5.30×10^{-10}	500	10 @ 600^{o}C	88
$Ba_3(Ca_{1.18}Nb_{1.82})O_9$	H^+	AgPd(C&A)	2.16×10^{-9}	620	X	89
YDC-$Ca_3(PO_4)_2$-K_3PO_4	H^+	AgPd(C&A)	6.95×10^{-9}	650	14 @ 600^{o}C	90
$La_{0.9}Sr_{0.1}Ga_{0.8}Mg_{0.2}O_{3-\delta}$	H^+	AgPd (C&A)	3.37×10^{-9}	550	X	91
$La_{0.9}Ba_{0.1}Ga_{0.8}Mg_{0.2}O_{3-\delta}$	H^+	AgPd (C&A)	1.89×10^{-9}	520	47 @ 800^{o}C	92
$BaCe_{0.85}Dy_{0.15}O_{3-\delta}$	H^+	AgPd(C&A)	3.5×10^{-9}	530	9.0 @ 600^{o}C	93
$BaCe_{0.2}Zr_{0.7}Y_{0.1}O_{2.9}$	H^+	Ni-BCZY27(C),Rh(A)	2.9×10^{-9}	550	X	94
Carbonate-$LiAlO_2$	H^+	Co_3Mo_3N (C),AgPd(A)	2.23×10^{-10}	400	X	70
Carbonate-$LiAlO_2$	H^+	Fe_3Mo_3N(C),AgPd(A)	1.88×10^{-10}	425	X	95
Carbonate-$LiAlO_2$	H^+	$CoFe_2O_4$-Ag(C),AgPd(A)	2.32×10^{-10}	400	X	96
$Ba_{0.5}Sr_{0.5}Ti_{0.9}Ru_{0.1}O_{3-\delta}$	H^+	BSTR(C),Ni-BCZY(A)	1.1×10^{-9}	500	X	97
$BaCe_{0.9}Ca_{0.1}O_{3-\delta}$	H^+	AgPd(C&A)	2.69×10^{-9}	480	X	98
$Ba(Ca_{1.18}Nb_{1.5})O_{9-\delta}$	H^+	AgPd(C&A)	1.42×10^{-9}	620	X	89
$Ba_3CaZr_{0.5}Nb_{1.5}O_{9-\delta}$	H^+	AgPd(C&A)	1.82×10^{-9}	620	X	89
$Ba_3Ca_{0.9}Nd_{0.28}Nb_{1.82}O_{9-\delta}$	H^+	AgPd(C&A)	2.16×10^{-9}	620	X	89
$BaCe_{0.9}Sm_{0.1}O_{3-\delta}$	H^+	AgPd(C&A)	5.23×10^{-9}	620	2.0 @ 600^{o}C	99
$BaCe_{0.8}Gd_{0.1}Sm_{0.1}O_{3-\delta}$	H^+	AgPd(C&A)	5.82×10^{-9}	620	5.0@ 600^{o}C	99
$Na_{0.5}K_{0.5}OH$ melt	H^+/N^{3-}	Fe_2O_3(C),Ni(A)	1×10^{-8}	200	X	100
NaOH-KOH melt	H^+/N^{3-}	Fe_2O_3/AC(C),Ni(A)	8.27×10^{-9}	250	X	101
NaOH-KOH melt	H^+/N^{3-}	Ni(Fe_3O_4)(C),Ni(A)	6.54×10^{-10}	255	X	102
LiCl-KCl-CsCl melt	H^+/N^{3-}	Ni(Fe_2O_3)(C),Li-Al(A)	3×10^{-10}	327	X	103
LiCl-KCl-CsCl melt	H^+/N^{3-}	Ni($CoFe_2O_4$)(C),Li-Al(A)	1.78×10^{-10}	327	X	103

X: conductivity values not reported

mol cm^{-2}s^{-1} as the temperature increased from 550 to 650 $^\circ C$. Another study using a symmetric Pt|GDC|Pt cell utilized a more conductive electrolyte, i.e. gadolinium doped ceria (GDC), and achieved a higher formation rate on the order of 10^{-11} mol cm^{-2}s^{-1} at 600$^\circ C$.[73] The low synthesis rates may be attributed to using water vapor as a hydrogen source. The synthesis rate was shown to increase significantly with the use of hydrogen to 10^{-9} mol cm^{-2}s^{-1} at 650$^\circ C$ using $Ce_{0.8}M_{0.2}O_{2-\delta}$ (doped with M=Gd, La, Y, or Sm)[74]. However, in this instance the doped cerates acted as proton conductors as opposed to oxygen conductors. Thus, the selection of H_2 or H_2O as a hydrogen source is non-trivial for both proton conducting and oxide conducting systems. Additionally, the $Ce_{0.8}M_{0.2}O_{2-\delta}$ doped cerates demonstrated a positive correlation between the ionic conductivity and the synthesis rate, further emphasizing the need for highly conductive electrolytes. Since oxygen and oxygen anions do not participate in the reaction mechanism for ammonia formation, a higher electrolyte conductivity should not adversely affect the faradaic efficiency. Recently, there have been numerous solid ion conductors which have been discovered that can effectively operate at lower temperatures. $Bi_2V_{1.9}Cu_{0.1}O_{5.35}$ (BiCuVOX) is an example of an electrolyte which can operate at 400$^\circ C$ with conductivities near 10^{-2} S cm^{-1}(Fig. 6).

3.1.4 Nitride Conducting Molten Electrolytes

Molten electrolytes are are typical eutectic mixtures of alkali chlorides or alkali hydroxides. Common examples of molten electrolytes include eutectic molten chloride salts (LiCl-KCl-CsCl) and eutectic molten hydroxides (NaOH-KOH). Molten electrolytes

employed in ammonia electrosynthesis typically have N^{3-} and H^+ ions as charge carriers and operate between 200-500°C.

Nitrogen is a reactant at the cathode and is reduced to nitride ions:

$$N_2 + 6e^- \longrightarrow 2N^{3-}$$

Hydrogen is oxidized at the anode and reacts with the nitride ions to produce ammonia:

$$3H_2 + 2N^{3-} \longrightarrow 2NH_3 + 6e^-$$

Water, methane (CH_4), hydrogen sulfide (H_2S), hydrochloric acid (HCl), and hydrogen gas (H_2) have all been used as reactants at the anode.[111]

Recently, a rate of $3*10^{-10}$mol cm^{-2}s^{-1} at 327°C was achieved in LiCl-KCl-CsCl molten chloride electrolyte[103]. The cell employed a Li-Al anode, Ni cathode, a hematite (Fe_2O_3) catalyst surface area. The nano-particles get reduced at the cathode and form an active Fe phase, which results in increase in the current density (e.g. synthesis rate). While the rate-limiting step in gas/vapor systems is the dissociation of nitrogen, molten salt electrolytes suffer from low N_2 dissolution.[112] The N_2 solubility can be improved via the addition of a nominal amount of an inorganic additive (e.g. Li_3N). A rate of 3.3×10^{-9} mol cm^{-2}s^{-1} at 400°C was demonstrated when 0.5mol% of Li_3N was dissolved into a LiCl-KCl-CsCl molten electrolyte[113]. Furthermore, when 0.5wt% of Li_3N was added to the LiCl-KCl cell a rate as high as 2×10^{-8} mol cm^{-2}s^{-1} at 300°C[112].

Hydroxide molten electrolytes operate at lower temperatures and are less corrosive than molten chloride electrolytes. However, they suffer from low Faradaic efficiencies because hydrogen evolution is thermodynamically favorable[114]. To suppress hydrogen evolution, it is common to disperse electrically conducting hematite particles (carbon coated Fe_2O_3) in the molten electrolyte. Carbon-coated hematite particles adsorb onto a stainless steel cathode more easily than that of uncoated hematite; resulting in an increased reduction of the particles to the more active Fe phase for nitrogen fixation. When a nickel anode was used, a synthesis rate of 8.27×10^{-9} mol cm^{-2}s^{-1} and faradaic efficiency of 4.9% at 250°C was observed using a NaOH-KOH molten electrolyte[101]. Table 1 summarizes the recent performances reported for molten electrolytes.

3.2 Intermediate Temperature Electrocatalyst and Electrodes

Although there are extensive studies on electrocatalyst materials for ambient electrosynthesis, there are significantly less investigations on elecrocatalysts for intermediate temperature electrosynthesis. While material selection for both low and intermediate temperature routes have a similar objective, there are some additional materials challenges when moving toward intermediate temperature systems. Namely, the electrocatalyst's chemical and physical stability at elevated temperatures and the electrocatalyst's chemical compatibility with the solid electrolyte are two significant challenges. Ideal catalyst materials maintain high electronic conductivity and have a minimal activation overpotential for the desired reaction (e.g. nitrogen reduction at cathode, hydrogen oxidation at anode). The catalyst in order to be selective, must also have a high activation overpotential for competing reactions. By having a high overpotential for an undesirable reaction, one can achieve high product selectivity.

Palladium has been demonstrated to be an efficient hydrogen trap that facilitates nitrogen reduction and suppresses desorption and formation of hydrogen gas[63,115,116]. The most widely investigated cathode catalyst for intermediate electrosynthesis is AgPd[63,117,118]. Rates of ammonia formation ranging from 10^{-10} to 10^{-8} mol cm^{-2}s^{-1} have been demonstrated for AgPd electrocatalysts and show high Faradaic efficiencies (50-80%) at intermediate temperatures (450-600°C)[31,76,89,91,92,119,120]. This differs from thermocatalytic reactors which typically achieve high production rates with Fe and Ru-based catalyst. Theoretical investigations suggest that the most active surfaces for nitrogen reduction are Fe, Ru, Mo and Rh[121] and early transition metals (Sc, Y, Ti and Zr) can bind N-adatoms stronger than H-adatoms. Thus, early transition metals that are present in the solid electrolyte (e.g. Zr) may play a role in suppressing side reactions. (e.g. hydrogen evolution). The high activity associated with the AgPd catalyst in intermediate ammonia electrosynthesis is likely due to complex interactions between the metal catalyst and constituents within the solid electrolyte (e.g. Ba, Ce, Zr).

Precious metal catalysts such as Pd, Ag, Ru, and Rh exhibit high electrocatalytic activity towards ammonia and have high electronic conductivity. However, due to cost concerns, there is significant interest in non-precious metal catalysts. Non-precious metal catalysts such as Fe, Mo, Co and Zr are currently being actively examined because of their cost and abundance. One major challenge with non-precious metal catalysts is low thermal stability and easily aggregated at elevated temperatures[122,123]. Noble metal nanoparticles with homogeneity in size, shape, and surface properties are potential catalysts for electrochemical ammonia synthesis by increasing electrochemical surface area (ECSA). The nanostructures of catalysts have been considered as an effective strategy at ambient circumstances. However, even noble metal nanoparticles are vulnerable at intermediate temperatures (up to 600 °C), which inevitably lead to loss of ECSA due to aggregation, Ostwald ripening, and sintering[124]. Another approach used to diminish catalyst poisoning is to employ Barium-type perovskite materials. Recently, $Sm_{0.6}Ba_{0.4}Fe_{0.8}Cu_{0.2}O_{3-\delta}$ was used as both cathode and anode and achieved ammonia formation rates of 9.19×10^{-7} mol cm^{-2}s^{-1} and 1.53×10^{-10} mol cm^{-2}s^{-1} for wet air and wet N_2, respectively[125].

Bimetallic and/or multi-component catalyst systems provide unique opportunities to tailor the binding energies of reactants, products, and intermediates (e.g. H_2, N_2, etc.). This level of control can aid in improving synthesis rates and suppressing side reactions. In thermocatalytic production of ammonia, metal promoters (e.g. Ba^+) in a Co/CeO_2 catalyst surface was shown to be an effective pathway for tailoring intermediate interactions and improve synthesis rate. Using N_2 and H_2 temperature programmed desorption experiments, it was shown the presence of a small amount of metal promoter (Barium) effectively increased the adsorption of N_2 and H_2[117]. High amount of the metal pro-

moter led to decreases in the H_2 adsorption and synthesis rate [117]. Furthermore, incorporation of a potassium metal promoter led to decreases in H_2 and N_2 adsorption and very low synthesis rates. Barium was also shown to be an effective metal promoter on $Ru/Sr_2Nb_2O_7$ catalyst [126]. Thus, metal promoters can effectively change the binding energy of the reactant, but also can affect the catalyst structure and morphological characteristics. Therefore, there are a number of open questions regarding the role that the solid-solid interface play in nitrogen adsorption and activation.

Further attempts to increase the ammonia formation rate without using precious metals has led to the use of bimetallic transition metal nitride catalysts (e.g. CoMoN and FeMoN), which have obtained rates on the order of 10^{-10} to 10^{-9} mol $cm^{-2}s^{-1}$ [44,60,127]. The appeal for these catalysts are attributed to their theoretically high activity, ability to suppress the competing hydrogen evolution reaction (HER), and relatively affordable costs. These catalysts follow a Mars-van Krevelen mechanism, which utilizes surfaces nitrogen atoms and subsequently nitrogen vacancies to reduce gaseous nitrogen. [128] Theoretical studies suggest ZrN, NbN, CrN, and VN may be active for nitrogen fixation [129,130], and although recent studies show that they are not catalytically active at ambient temperatures [131 132], these have not been investigated under intermediate temperature cells.

Catalyst activity and electrode microstructure can influence electrosynthesis of ammonia. The membrane electrode assembly utilized for intermediate electrosynthesis of ammonia is comprised of a solid electrolyte sandwiched between two electrodes. The electrode may be the catalyst or a composite material composed of a mixed ionic-electronic conductors (MIEC) decorated with an electrocatalyst. The MIEC can provide a porosity to the electrode for effective gas transport while increasing the accessible surface area. Furthermore, the mixed ion electron conductor creates triple phase boundaries within the electrode structure where ion, electron, and reactant transport occurs (e.g. active sites). The structure (e.g. porosity) can be effectively altered via introducing pore formers during the processing step. Common MIECs include $Ba_{0.5}Sr_{0.5}Co_{0.8}Fe_{0.2}O_{3-\alpha}$ (BSCF) with Fe doping [81], $La_{0.6}Sr_{0.4}Co_{0.2}Fe_{0.8}O_{3-\alpha}$ (LSCF) with Fe doping [83], and Ni-$BaCe_{0.9}Y0_{.1}Ru_xO_3$ (x=10,20) (Ni-BCYR) with Ru doping [133]. Dopant materials with high electronic conductivity and activity are desirable. Iron doped MIECs tend to achieve higher formation rates (synthesis rates) than ruthenium-based MIECs when tested under similar operating conditions. For example, a BSCF (Fe-based) electrode [81] tested in a wet H_2/dry N_2 atmosphere near 500 $^{\circ}C$ achieved $\sim$8x higher rate of ammonia formation than Ni-BCYR (Ru-based) electrode [88]. Similarly, a LSCF (Fe-based) electrode [83] showed better performance than a Ni-BCYR (Ru-based) catalyst electrode [133].

Molten electrolytes tend to use catalysts that differ from those used in solid state electrolytes. The ammonia electrosynthesis rate in a molten chloride electrolyte was highest with cobalt and/or nickel catalysts, and lowest with titanium and iron catalysts [134]. The catalyst's wettability and electrical properties within the molten salt greatly impacts its performance. Non-wetting catalysts cannot interact with dissolved nitrogen and thus have lower activities. In another study nickel was implemented as the working electrode and Fe_2O_3 and $CoFe_3O_4$ nano particles served as the catalysts [103]. Introducing nanoparticles into the molten electrolyte can expand the active sites beyond the nickel electrocatalyst. Specifically, there are active sites between the electrode|nanoparticle and the nanoparticle itself that can serve as active sites for nitrogen reduction.

Therefore, there is a significant need to develop and study catalyst and electrodes for intermediate temperature ammonia electrosynthesis. Catalyst and dopants are needed which are highly conductive and active for nitrogen fixation. Furthermore, the interactions between the catalyst and the solid electrolyte need to be investigated to understanding the role of transition metals within the solid electrolytes. High thermal and mechanical stability are necessary, but structure-sensitive resistance to poisoning should be also considered for long lifetime productions. Finally, cost must be considered when choosing a catalyst, as a large portion of the capitol cost is associated with the nitrogen reduction catalyst and the solid electrolytes.

3.3 Future directions for solid electrolytes and catalyst

Continued progress in this field is dependent on addressing key limitations for these electrochemical cells. Catalysts needs to improve their selectivity and activity, but current catalysts are still plagued by the competing hydrogen evolution reaction (HER) and the slow reduction of nitrogen. Both of these limitations could be mitigated by implementing an intermediary for hydrogen and nitrogen on current catalysts. For example, an amalgam of lithium and iron is shown to dissociate nitrogen more effectively than using solely iron and improve the hydrogen surface coverage. [135] Additionally, MIECs remain a viable option for improving the activity as long as optimal dopants are chosen. Further enhancement of the MIECs would involve exsolving the dopant and shrinking its particle size during the reduction process, a method previously shown to improve the synthesis rate [133].

Oxide ion and proton-conducting materials such as perovskites are one of the candidates for replacement of noble PdAg catalyst. Recently, Fop et al. reported $Ba_7Nb_4MoO_{20}$ hexagonal perovskites showed high proton and oxide ion conductivity at 510 °C (bulk conductivity is 4.0 mS cm^{-1}) [136]. $Ba_7Nb_4MoO_{20}$ also exhibited excellent chemical and electrochemical stability. They have discovered several notable ion conductivity of $Ba_3NbMO_{8.5}$ (M = Mo, W). Intermediate temperature (300-600 °C) proton conducting materials have been reported numerous structural families that may contribute to generating ammonia [137–140].

Ideally, electrolytes should have high ionic conductivity at elevated temperatures within 100 to 400°C to minimize the decomposition of ammonia. Currently the most promising electrolytes that fit this criteria are the solid acid electrolytes and the carbonate-based composites. However, multiple ions migrate throughout these electrolytes resulting in a reduced protonic conductivity. Thus, sufficient conductivity and transference number are both desirable. A new type of promising proton conductor is based on lithium super conducting electrolytes (LISICON). A $Li_{13.9}Sr_{0.1}Zn(GeO_4)_4$ can undergo ion-exchange in acid to form a proton conductor that has an ionic conductivity above that of

many perovskite-structured proton conductors (0.048 S cm^{-1}).[45] This indicates that many other alkali-conducting electrolytes may be converted to conduct protons to synthesize ammonia effectively.

4 Measurement Issues

4.1 Ammonia Measurements

Ammonia is measured using colorimetric assays[141], ion chromatography[142], fluorescence[143,144], ion selective electrodes[145], and H1-NMR spectroscopy[146]. Colorimetric methods utilize UV-vis spectrometer to detect indophenol blue dye formed through a reaction between ammonia and chemical reagents (e.g. NaOH, salicylic acid)[141]. Ionic chromatography utilizes ion-exchange columns to separate ammonium ions from other ions in solutions, and then detects ammonium concentration through a conductivity detector. In fluorescence-based spectroscopy, reagents react with ammonia species to form fluorescence. The ammonia concentration is correlated to the degree of emitted fluorescence[143,144]. Ion selective electrodes are type of sensors that convert the specific activity of ammonium ion dissolved in the solution into an electrical potential[145]. H1 NMR uses a magnetic fields to determine and distinguish the nuclei spin of a proton on ammonia[146].

Each measurement method has the propensity to produce a degree of error depending on the testing conditions. One way error can be introduced is if there are signal interferences (ions, transition metals, sacrificial agents). Ions such as PO_4^{3-}, SO_4^{2-}, Ca^{2+}, Mg^{2+} and transition metals such as Ru^{3+}, Ce^{3+}, Fe^{2+} interfere withe Nesslers' reagent and indophenol blue methods[147,148]. Alcohol based species also interfere with Nesslers' reagent resulting an overestimation of ammonia concentration, whereas the presence of alcohol can result in underestimated ammonia concentration with indophenol blue method[147,149,150]. Common interferants for ionic chromatography include Li^+ and Na^+[151]. The close retention time among these ions and ammonium leads to separation difficulty, especially when the produced ammonia concentrations are much lower than these alkali ions. Ion chromatography is also very sensitive to concentration, and therefore ammonia can not be easily detected if the supporting electrolyte is high concentration, which is common for aqueous electrochemical systems. Ion selective electrode is sensitive to the presence of akali and akaline earth ions, which act as interferences leading to inaccurate ammonia concentration data[152]. Certain organic solvent (e.g. acentonitrile, trifluorotoluene) may cause interference with H1-NMR, through peak overlapping. Therefore, it is common to add maleic acid as an internal standard to reduce the peak overlap with H1-NMR[153].

Contamination such as adventitious ammonia and NOx also impact the accuracy to each measurement method. Nitrogen gas cylinders often contain trace amount of NOx and/or ammonia which can result in a certain concentration of ammonia which does not arise through nitrogen fixation. To overcome this challenge, acid or copper/ethanol catalyst traps are used prior to the reactor system to minimize contamination[146,154]. Nitrogen in plastic tubing, tape, connections, and even the reactor may also introduce contamination. Proton exchange membranes without proper cleaning can also store ammonium through ion exchange process[151]. Nitrogen-based and carbon-based catalysts could easily chemisorb ammonia species without repetitive washing prior to the tests[147]. Catalysts such as g-C_3N_4 can deteriorate, resulting in a another potential source of ammonia contamination[147,155]. Similarly, the as-prepared Sn(II) phthalocyanine has a false-positives results in which the detected ammonia concentration were higher in control experiments (Ar) than N_2[8]. Therefore, because of the ease of contamination that can occur before during or after the experiments, researchers are rapidly moving forward using isotope labeling gases (N14, N15) coupled with H1-NMR to distinguish the produced ammonia from other contaminated ammonia sources[153,156–158]. Rarely studies on intermediate and high-temperature electrocatalytic ammonia synthesis have utilized isotope labeled N15 tests to validate the produced ammonia concentrations (Table 1). Therefore, a recommendation for N15 validation is required.

Another factor that may lead to erroneous results is pH value of the samples. Indophenol blue methods provide accurate ammonia concentration when the resulted pH after addition of chemical reagents (e.g. 1 M NaOH) are in pH range from 7-13[147,151]. In acidic environment (pH = 4-6) the detected ammonia concentration was significantly affected. For Nessler's Reagent, ammonia concentration are accurate in acidic, neutral and alkaline conditions. Though ammonia concentration is not accurate in certain pH range, with appropriate calibration curve, the entirely reliable results can be obtained in the pH range of 1-13 of the samples of nitrogen reduction tests before addition of chemical reagents for both indophenol blue and Nesslers Reagent methods[153]. Ionic chromatography is often deemed the most accurate approach for measuring ammonia, especially in acidic and neutral environments. H1-NMR is deemed to be the most robust method, yet pH can impact H1-NMR as well. It is common to add small amount of acid (e.g. H_2SO_4) into the samples for measurement because ammonia are stable in acidic media[146,157]. However, too low of the pH value may leads to erroneous results. Report showed that the H_2SO_4 concentration of the final samples in the range of 0.02 - 0.2 M[153] would have accurate ammonia concentration data. Other challenges of H1-NMR is the high costs of isotope labeling gas, locking solvents (DMSO-d_6) and NMR tubes. A most recent study uses a relative cheaper material (dansyl chloride), faster measuring time (3.5 mins) with a more widely used analytical measurement method (mass spectrometer)[158] by coupling isotope labeling gas with ultrahigh performance liquid chromatography mass spectrometry (UPLC-MS). However, pH value of the samples is still an issue we need to be careful.

4.2 System operating current

One way to eliminate the challenges with measuring ammonia is to generate more product experimentally to minimize error. This can be accomplished through running experiments at higher current density or for longer periods of time. This can aid in moving production values well beyond the limit of detection (LOD) where error is unlikely to play a large role in measurement (Fig. 7).

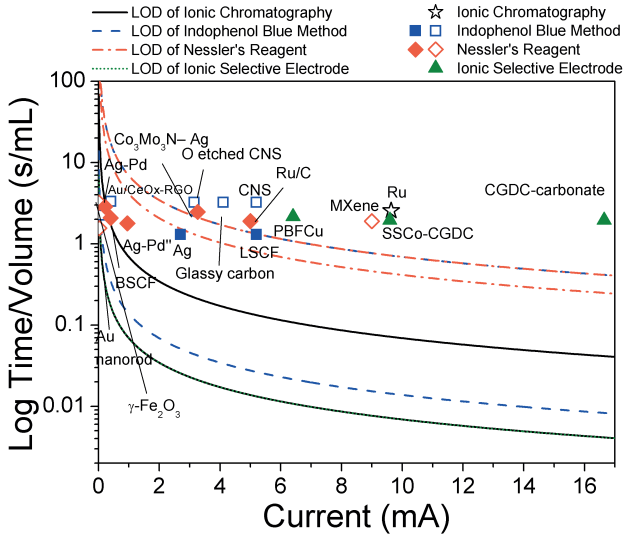

Fig. 7 Limit of Detection for low (hollow symbols)[105,159–164] and intermediate temperature (solid symbols) ammonia electrosynthesis[38,60,82,96,120,165–167]

The LOD is defined as the lowest quantitative number of a substance that can be distinguished by absence of that substance[168]. The Nessler's reagent LOD is 0.6 - 1 ppm[169],the indophenol blue method LOD is 0.02 - 1 ppm[169–172], ion chromatography LOD of 0.01 - 0.1 ppm, ion selective electrodes LOD of 0.01 ppm, fluorescence has a LOD of 0.01-0.07ppm[143,144] and H1-NMR has a LOD of 0.05-0.17 ppm[153,156]. Typically, most experimentalist are only measuring ammonia concentrations on the order or 1 ppm or less, and are operating with current around 1-5 mA (Fig. 7). Most experimentalist will aim to minimize the volume of electrolyte to concentrate the ammonia faster, but there is a limited volume which one can operate in due to sample volume requirements.

Low temperature ammonia electrosynthesis for the most part remain near or at the LOD (e.g.Ru, CNS,O-etched CNS, MXene and Glassy Carbon)[105,159,160]. Some reports are even below the LOD (e.g.γ Fe_2O_3, Au-TiO_2 nanoclusters, Amporphous Au on CeOx/RGO and Au nanorod)[161–164]. Intermediate temperature ammonia electrosynthesis demonstrations also have reported some data above LOD (Ru/C, PBFCu, Co_3Mo_3N-Ag, CGDC-carbonate, SSCo-CGDC)[38,60,165]. However, most intermediate temperature demonstrations also fall near or below LOD (i.e. AgPd, Ag, LSCF, and BSCF)[82,96,120,166,167].Due to the interferant ions and unavoidable contamination, it is not ideal to report ammonia concentrations which are near or below the LOD. The clear and easiest way to move beyond the limit of detection is to increase the current and increase the time of the test. Therefore, we advocate for the use of multiple measurements techniques, high current testing, and proper use of statistics to confirm all ammonia measurements.

5 Conclusions and Outlook

There is tremendous potential for advances in intermediate temperature ammonia electrosynthesis. The higher temperature operation, open the doors to achieve unprecedented rates of production and energy efficiencies which may be capable of competing with thermocatalytic approaches. Furthermore, these projected performance values are not attainable with low temperature electrochemical routes. In order to achieve the potential benefits there is a tremendous need to develop intermediate temperature solid electrolytes capable of conducting protons or oxygen-ions, as current solid electrolytes are responsible for most ohmic losses within the cell. Furthermore, there is a need to not only design selective catalyst, but to understand the role of the solid-solid interface and interphase may play on nitrogen electrocatalyst. Finally, as researchers begin to explore this potential direction, care must be taken to understand what analytical measurement technique is capable of quantify produced ammonia. Ultimately, all measurements should be corroborated through multiple techniques, and care should be taken to design experiments which move well beyond the limit of detection of each measurement technique.

Conflicts of interest

In accordance with our policy on Conflicts of interest please ensure that a conflicts of interest statement is included in your manuscript here. Please note that this statement is required for all submitted manuscripts. If no conflicts exist, please state that "There are no conflicts to declare".

Acknowledgements

This material is based upon work supported by the National Science Foundation under Grant No.184661 and No.1933646.

Notes and references

1 G. Soloveichik, *Nature Catalysis*, 2019, **2**, 377.
2 A. R. Singh, B. A. Rohr, J. A. Schwalbe, M. Cargnello, K. Chan, T. F. Jaramillo, I. Chorkendorff and J. K. Nørskov, *ACS Catalysis*, 2017, **7**, 706–709.
3 A. J. Medford and M. C. Hatzell, *ACS Catalysis*, 2017, **7**, 2624–2643.
4 R. Hawtof, S. Ghosh, E. Guarr, C. Xu, R. M. Sankaran and J. N. Renner, *Science advances*, 2019, **5**, eaat5778.
5 A. J. Martín, T. Shinagawa and J. Pérez-Ramírez, *Chem*, 2019, **5**, 263–283.
6 P. Mehta, P. Barboun, F. A. Herrera, J. Kim, P. Rumbach, D. B. Go, J. C. Hicks and W. F. Schneider, *Nature Catalysis*, 2018, **1**, 269.
7 A. Vorotto, *Raising the Standards: Enhanced Catalytic Performance for Global Ammonia Production.*
8 M. A. Shipman and M. D. Symes, *Catalysis Today*, 2017, **286**, 57–68.
9 C. Chen, H. Aryafar, G. Warrier, K. M. Lovegrove and A. S. Lavine, AIP Conference Proceedings, 2016, p. 050010.
10 M. Reese, C. Marquart, M. Malmali, K. Wagner, E. Buchanan, A. McCormick and E. L. Cussler, *Industrial & Engineering Chemistry Research*, 2016, **55**, 3742–3750.
11 A. Allman, P. Daoutidis, D. Tiffany and S. Kelley, *AIChE Journal*, 2017, **63**, 4390–4402.
12 Z. J. Schiffer and K. Manthiram, *Joule*, 2017, **1**, 10–14.
13 O. Schmidt, A. Gambhir, I. Staffell, A. Hawkes, J. Nelson and

S. Few, *International Journal of Hydrogen Energy*, 2017, **42**, 30470–30492.
14 A. Hauch, S. D. Ebbesen, S. H. Jensen and M. Mogensen, *Journal of Materials Chemistry*, 2008, **18**, 2331–2340.
15 C. C. McCrory, S. Jung, I. M. Ferrer, S. M. Chatman, J. C. Peters and T. F. Jaramillo, *Journal of the American Chemical Society*, 2015, **137**, 4347–4357.
16 K. Noelker and J. Ruether, Nitrogen+ Syngas Conference, 2011.
17 D. A. Salvatore, D. M. Weekes, J. He, K. E. Dettelbach, Y. C. Li, T. E. Mallouk and C. P. Berlinguette, *ACS Energy Letters*, 2017, **3**, 149–154.
18 Y. Guo, H. Yang, X. Zhou, K. Liu, C. Zhang, Z. Zhou, C. Wang and W. Lin, *Journal of Materials Chemistry A*, 2017, **5**, 24867–24873.
19 V. Gurau, F. Barbir and H. Liu, *Journal of The Electrochemical Society*, 2000, **147**, 2468–2477.
20 C. Chen and G. Ma, *Journal of Alloys and Compounds*, 2009, **485**, 69–72.
21 D. Higgins, C. Hahn, C. Xiang, T. F. Jaramillo and A. Z. Weber, *ACS Energy Letters*, 2018, **4**, 317–324.
22 S. Giddey, S. Badwal and A. Kulkarni, *International Journal of Hydrogen Energy*, 2013, **38**, 14576–14594.
23 S. Hossain, A. M. Abdalla, S. N. B. Jamain, J. H. Zaini and A. K. Azad, *Renewable and Sustainable Energy Reviews*, 2017, **79**, 750–764.
24 G. Qing, R. Ghazfar, S. T. Jackowski, F. Habibzadeh, M. M. Ashtiani, C.-P. Chen, M. R. Smith III and T. W. Hamann, *Chemical Reviews*, 2020.
25 D. Yi, S. Sanghvi, C. P. Kowalski and S. M. Haile, *Chemistry of Materials*, 2019, **31**, 9807–9818.
26 S. M. Haile, G. Staneff and K. H. Ryu, *Non-stoichiometry, grain boundary transport and chemical stability of proton conducting perovskites*, 5, 2001.
27 S. M. Haile, C. R. Chisholm, K. Sasaki, D. A. Boysen and T. Uda, *Faraday discussions*, 2007, **134**, 17–39.
28 S. Sanghvi and S. M. Haile, *Solid State Ionics*, 2020, **349**, 115291.
29 I. A. Amar, R. Lan, C. T. Petit and S. Tao, *Journal of Solid State Electrochemistry*, 2011, **15**, 1845–1860.
30 S. Hossain, A. M. Abdalla, S. N. B. Jamain, J. H. Zaini and A. K. Azad, *Renewable and Sustainable Energy Reviews*, 2017, **79**, 750–764.
31 I. Garagounis, V. Kyriakou, A. Skodra, E. Vasileiou and M. Stoukides, *Frontiers in Energy Research*, 2014, **2**, 1.
32 J. Kim, S. Sengodan, S. Kim, O. Kwon, Y. Bu and G. Kim, *Renewable and Sustainable Energy Reviews*, 2019, **109**, 606–618.
33 S. M. Haile, D. A. Boysen, C. R. Chisholm and R. B. Merle, *Nature*, 2001, **410**, 910–913.
34 S. M. Haile, *Materials Today*, 2003, **6**, 24–29.
35 C. R. Chisholm, D. A. Boysen, A. B. Papandrew, S. K. Zecevic, S. Cha, K. A. Sasaki, Á. Varga, K. P. Giapis and S. M. Haile, *Interface*, 2009, **18**, 53–59.
36 G. Qing, R. Kikuchi, A. Takagaki, T. Sugawara and S. T. Oyama, *Journal of Power Sources*, 2016, **306**, 578–586.
37 T. Matsui, T. Kukino, R. Kikuchi and K. Eguchi, *Journal of The Electrochemical Society*, 2006, **153**, A339–A342.
38 S. Kishira, G. Qing, S. Suzu, R. Kikuchi, A. Takagaki and S. T. Oyama, *International Journal of Hydrogen Energy*, 2017, **42**, 26843–26854.
39 C. R. I. Chisholm, D. a. Boysen, A. B. Papandrew, S. Zecevic and S. Cha, *From Laboratory Breakthrough to Technological Realization: The Development Path for Solid Acid Fuel Cells*, Fall, 2009.
40 A. Paw, C. Pawlaczyk, B. Hilczer *et al.*, *Solid State Ionics*, 1990, **44**, 17–19.
41 C. Ramasastry and K. S. Ramaiah, *Journal of Materials Science*, 1981, **16**, 2011–2016.
42 K. Imamura and J. Kubota, *Sustainable Energy & Fuels*, 2018, **2**, 1278–1286.
43 K. Sato, K. Imamura, Y. Kawano, S.-i. Miyahara, T. Yamamoto, S. Matsumura and K. Nagaoka, *Chemical science*, 2017, **8**, 674–679.
44 I. A. Amar, R. Lan, C. T. G. Petit and S. Tao, *Electrocatalysis*, 2015, **6**, 286–294.
45 M. Liu, Y. Chen, L. A. Zhang, T. Wei and P. Yang, *Chemistry of Materials*, 2017, **29**, 1490–1495.
46 S. J. Skinner and J. A. Kilner, *Review Literature And Arts Of The Americas*, 2003, **6**, 30–37.
47 S. Choi, C. J. Kucharczyk, Y. Liang, X. Zhang, I. Takeuchi, H. I. Ji and S. M. Haile, *Nature Energy*, 2018, **3**, 202–210.
48 B. C. Steele, *Solid State Ionics*, 2000, **129**, 95–110.
49 D. W. Strickler and W. G. Carlson, *Journal of the American Ceramic Society*, 1965, **48**, 286–289.
50 K.-D. Kreuer, *Annual Review of Materials Research*, 2003, **33**, 333–359.
51 Y. Yamazaki, F. Blanc, Y. Okuyama, L. Buannic, J. C. Lucio-Vega, C. P. Grey and S. M. Haile, *Nature materials*, 2013, **12**, 647–651.
52 L. Malavasi, C. A. Fisher and M. S. Islam, *Chemical Society Reviews*, 2010, **39**, 4370–4387.
53 K. D. Kreuer, *Aspects of the formation and mobility of protonic charge carriers and the stability of perovskite-type oxides*, 1, 1999.
54 C.-H. Kim and C. D. Frisbie, *Journal of the American Chemical Society*, 2016, **138**, 7220–7223.
55 A. Khorshidi, J. Violet, J. Hashemi and A. A. Peterson, *Nature Catalysis*, 2018, **1**, 263–268.
56 M. A. Ardagh, O. A. Abdelrahman and P. J. Dauenhauer, *ACS Catalysis*, 2019, **9**, 6929–6937.
57 G. Pitselis, P. Petrolekas and C. Vayenas, *Ionics*, 1997, **3**, 110–116.
58 G. Marnellos, S. Zisekas and M. Stoukides, *Journal of Catalysis*, 2000, **193**, 80–87.
59 C. Yiokari, G. Pitselis, D. Polydoros, A. Katsaounis and C. Vayenas, *The Journal of Physical Chemistry A*, 2000, **104**, 10600–10602.

60 J. Díez-Ramírez, V. Kyriakou, I. Garagounis, A. Vourros, E. Vasileiou, P. Sánchez, F. Dorado and M. Stoukides, *ACS Sustainable Chemistry & Engineering*, 2017, **5**, 8844–8851.

61 K. Kreuer, W. Münch, M. Ise, T. He and A. Fuchs, *Berichte der Bunsen-Gesellschaft*, 1997, **101**, 1344–1350.

62 P. Berger, F. Mauvy, J. Grenier, N. Sata, A. Magrasó, R. Haugsrud and P. Slatere, *Proton-Conducting Ceramics*, Pan Stanford, 2015, pp. 24–95.

63 G. Marnellos, C. Athanasiou and M. Stoukides, *Evaluation and use of the Pd | SrCe0.95Yb0.05O3| Pd electrochemical reactor for equilibrium-limited hydrogenation reactions*, 1-2, 1998.

64 S. Zisekas, G. Karagiannakis, G. Marnellos and M. Stoukides, *Ionics*, 2002, **8**, 118–122.

65 X. T. L. SU, R. Quan and J. D. WANG, *Acta Chimica Sinica*, 2003, **4**, year.

66 Y. Guo, B. Liu, Q. Yang, C. Chen, W. Wang and G. Ma, *Electrochemistry Communications*, 2009, **11**, 153–156.

67 Y. H. Xie, J. D. Wang, R. Q. Liu, X. T. Su, Z. P. Sun and Z. J. Li, *Solid State Ionics*, 2004, **168**, 117–121.

68 B. H. Wang, J. De Wang, R. Liu, Y. H. Xie and Z. J. Li, *Journal of Solid State Electrochemistry*, 2005, **11**, 27–31.

69 B. Wang, R. Liu, J. Wang, Z. Li and Y. Xie, *Chinese Journal of inorganic chemistry*, 2005, **21**, 1551–1555.

70 I. A. Amar, R. Lan, C. T. Petit, V. Arrighi and S. Tao, *Solid State Ionics*, 2011, **182**, 133–138.

71 G. J. JANZ and M. R. LORENZ, *Journal of chemical and Engineering data*, 1961, **6**, 321–323.

72 A. Skodra and M. Stoukides, *Solid State Ionics*, 2009, **180**, 1332–1336.

73 H. Jeoung, J. N. Kim, C. Y. Yoo, J. H. Joo, J. H. Yu, K. C. Song, M. Sharma and H. C. Yoon, *Korean Chemical Engineering Research*, 2014, **52**, 58–62.

74 R. Q. Liu, Y. H. Xie, J. D. Wang, Z. J. Li and B. H. Wang, *Solid State Ionics*, 2006, **177**, 73–76.

75 M. Ouzounidou, A. Skodra, C. Kokkofitis and M. Stoukides, *Solid State Ionics*, 2007, **178**, 153–159.

76 X. Wang, J. Yin, J. Xu, H. Wang and G. Ma, *Chinese Journal of Chemistry*, 2011, **29**, 1114–1118.

77 M. Zhang, J. Xu and G. Ma, *Journal of Materials Science*, 2011, **46**, year.

78 S. Klinsrisuk and J. T. Irvine, *Catalysis Today*, 2017, **286**, 41–50.

79 E. Vasileiou, V. Kyriakou, I. Garagounis, A. Vourros and M. Stoukides, *Solid State Ionics*, 2015, **275**, 110–116.

80 J. Yin, X. Wang, J. Xu, H. Wang, F. Zhang and G. Ma, *Solid State Ionics*, 2011, **185**, 6–10.

81 W. B. Wang, X. B. Cao, W. J. Gao, F. Zhang, H. T. Wang and G. L. Ma, *Journal of Membrane Science*, 2010, **360**, 397–403.

82 Y.-H. Xie, J.-D. Wang, R.-Q. Liu, X.-T. Su, Z.-P. Sun and Z.-J. Li, *Solid State Ionics*, 2004, **168**, 117–121.

83 D. S. Yun, J. H. Joo, J. H. Yu, H. C. Yoon, J. N. Kim and C. Y. Yoo, *Journal of Power Sources*, 2015, **284**, 245–251.

84 V. Kyriakou, I. Garagounis, A. Vourros, E. Vasileiou and M. Stoukides, *Joule*, 2020, **4**, 142–158.

85 Z. Lei, J. Jing, J. Pang, R. Hu, X. Shi, Z. Yang and S. Peng, *International Journal of Hydrogen Energy*, 2020, **45**, 8041–8051.

86 F. Kosaka, T. Nakamura, A. Oikawa and J. Otomo, *ACS Sustainable Chemistry & Engineering*, 2017, **5**, 10439–10446.

87 N. ShimodaMetal-organic framework-derived nitrogen-doped highly disordered carbon for electrochemical ammonia synthesis using N2and H2O in alkaline electrolytes, Y. Kobayashi, Y. Kimura, G. Nakagawa and S. Satowaka, *Journal of the Ceramic Society of Japan*, 2017, **125**, 252–256.

88 Y. Kobayashi, N. Shimoda, Y. Kimura and S. Satokawa, *ECS Transactions*, 2017, **75**, 43–52.

89 Z. J. Li, R. Q. Liu, Y. H. Xie, S. Feng and J. D. Wang, *Solid State Ionics*, 2005, **176**, 1063–1066.

90 B. H. Wang, J. D. Wang, R. Q. Liu, Y. H. Xie and Z. J. Li, *Journal of Solid State Electrochemistry*, 2006, **11**, 27–31.

91 F. Zhang, Q. Yang, B. Pan, R. Xu, H. Wang and G. Ma, *Materials Letters*, 2007, **61**, 4144–4148.

92 C. Chen and G. Ma, *Journal of Materials Science*, 2008, **43**, 5109–5114.

93 W. B. Wang, J. W. Liu, Y. D. Li, H. T. Wang, F. Zhang and G. L. Ma, *Solid State Ionics*, 2010, **181**, 667–671.

94 E. Vasileiou, V. Kyriakou, I. Garagounis, A. Vourros, A. Manerbino, W. G. Coors and M. Stoukides, *Topics in Catalysis*, 2015, **58**, 1193–1201.

95 I. A. Amar, R. Lan, C. T. Petit and S. Tao, *International Journal of Electrochemical Science*, 2014, **10**, 3757–3766.

96 I. A. Amar, C. T. Petit, G. Mann, R. Lan, P. J. Skabara and S. Tao, *international journal of hydrogen energy*, 2014, **39**, 4322–4330.

97 H. Kim, Y. S. Chung, T. Kim, H. Yoon, J. G. Sung, H. K. Jung, W. B. Kim, L. B. Sammes and J. S. Chung, *Solid State Ionics*, 2019, **339**, 115010.

98 J. Liu, Y. Li, W. Wang, H. Wang, F. Zhang and G. Ma, *Journal of Materials Science*, 2010, **45**, 5860–5864.

99 Z. Li, R. Liu, J. Wang, Z. Xu, Y. Xie and B. Wang, *Science and Technology of Advanced Materials*, 2007, **8**, 566.

100 F.-F. Li and S. Licht, *Inorganic Chemistry*, 2014, **53**, 10042–10044.

101 B. Cui, J. Zhang, S. Liu, X. Liu, W. Xiang, L. Liu, H. Xin, M. J. Lefler and S. Licht, *Green Chemistry*, 2016, **19**, 298.

102 Y. Bicer and I. Dincer, *Journal of The Electrochemical Society*, 2017, **164**, H5036–H5042.

103 K. Kim, C. Y. Yoo, J. N. Kim, H. C. Yoon and J. I. Han, *Korean Journal of Chemical Engineering*, 2016, **33**, 1777–1780.

104 G. Xu, R. Liu and J. Wang, *Science in China, Series B: Chemistry*, 2009, **52**, 1171–1175.

105 V. Kordali, G. Kyriacou and C. Lambrou, *Chemical Communications*, 2000, 1673–1674.

106 Y. Ren, C. Yu, X. Tan, X. Han, H. Huang, H. Huang and J. Qiu, *Small Methods*, 2019, **3**, year.

107 M. Li, H. Huang, J. Low, C. Gao, R. Long and Y. Xiong, *Small Methods*, 2019, **3**, year.

108 C. Duan, J. Tong, M. Shang, S. Nikodemski, M. Sanders, S. Ricote, A. Almansoori and R. O'Hayre, *Science*, 2015, **349**, 1321–1326.

109 E. D. Wachsman and K. T. Lee, *Science*, 2011, **334**, 935–939.

110 K. S. Lee, S. Maurya, Y. S. Kim, C. R. Kreller, M. S. Wilson, D. Larsen, S. E. Elangovan and R. Mukundan, *Energy and Environmental Science*, 2018, **11**, 979–987.

111 J. Yang, W. Weng and W. Xiao, *Journal of Energy Chemistry*, 2020, **43**, 195–207.

112 T. Murakami, T. Nishikiori, T. Nohira and Y. Ito, *Journal of The Electrochemical Society*, 2005, **152**, D75.

113 T. Murakami, T. Nishikiori, T. Nohira and Y. Ito, *Journal of the American Chemical Society*, 2003, **125**, 334–335.

114 S. Licht, B. Cui, B. Wang, F. F. Li, J. Lau and S. Liu, *Science*, 2014, **345**, 637–640.

115 G. Marnellos, C. Athanasiou, P. Tsiakaras and M. Stoukides, *Ionics*, 1996, **2**, 412–420.

116 E. Panagos, I. Voudouris and M. Stoukides, *Chemical engineering science*, 1996, **51**, 3175–3180.

117 B. Lin, Y. Liu, L. Heng, J. Ni, J. Lin and L. Jiang, *Journal of Rare Earths*, 2018.

118 S. Dahl, A. Logadottir, C. J. Jacobsen and J. K. Norskov, *Electronic factors in catalysis: The volcano curve and the effect of promotion in catalytic ammonia synthesis*, 1-2, 2001.

119 C. Y. Yoo, J. H. Park, K. Kim, J. I. Han, E. Y. Jeong, C. H. Jeong, H. C. Yoon and J. N. Kim, *ACS Sustainable Chemistry and Engineering*, 2017, **5**, 7972–7978.

120 W. Wang, X. Cao, W. Gao, F. Zhang, H. Wang and G. Ma, *Journal of Membrane Science*, 2010, **360**, 397–403.

121 E. Skúlason, T. Bligaard, S. Gudmundsdóttir, F. Studt, J. Rossmeisl, F. Abild-Pedersen, T. Vegge, H. Jónsson and J. K. Nørskov, *Physical Chemistry Chemical Physics*, 2012, **14**, 1235–1245.

122 C. N. Satterfield, *Heterogeneous catalysis in practice*, McGraw-Hill New York, 1980, vol. 416.

123 K. Wang, D. Smith and Y. Zheng, *Carbon Resources Conversion*, 2018, **1**, 2–31.

124 Z. Dai, S. Sun and Z. Wang, *Nano Letters*, 2001, **1**, 443–447.

125 R. Lan, K. A. Alkhazmi, I. A. Amar and S. Tao, *Faraday discussions*, 2015, **182**, 353–363.

126 M. Chen, M. Yuan, J. Li and Z. You, *Applied Catalysis A: General*, 2018, **554**, 1–9.

127 I. A. Amar, R. Lan, C. T. Petit and S. Tao, *Electrocatalysis*, 2015, **6**, 286–294.

128 C. D. Zeinalipour-Yazdi, J. S. Hargreaves and C. R. A. Catlow, *Journal of Physical Chemistry C*, 2015, **119**, 28368–28376.

129 Y. Abghoui and E. Skúlasson, *Procedia Computer Science*, 2015, **51**, 1897–1906.

130 Y. Abghoui, A. L. Garden, J. G. Howalt, T. Vegge and E. Skúlason, *Acs Catalysis*, 2015, **6**, 635–646.

131 B. Hu, M. Hu, L. Seefeldt and T. L. Liu, *ACS Energy Letters*, 2019, **4**, 1053–1054.

132 H.-L. Du, T. R. Gengenbach, R. Hodgetts, D. R. MacFarlane and A. N. Simonov, *ACS Sustainable Chemistry & Engineering*, 2019, **7**, 6839–6850.

133 F. Kosaka, T. Nakamura and J. Otomo, *Journal of The Electrochemical Society*, 2017, **164**, F1323–F1330.

134 K. Kim, J. N. Kim, H. C. Yoon and J. I. Han, *International Journal of Hydrogen Energy*, 2015, **40**, 5578–5582.

135 P. Wang, F. Chang, W. Gao, J. Guo, G. Wu, T. He and P. Chen, *Nature chemistry*, 2017, **9**, 64.

136 S. Fop, K. S. McCombie, E. J. Wildman, J. M. Skakle, J. T. Irvine, P. A. Connor, C. Savaniu, C. Ritter and A. C. Mclaughlin, *Nature materials*, 2020, 1–6.

137 X. Yang, A. J. Fernández-Carrión, J. Wang, F. Porcher, F. Fayon, M. Allix and X. Kuang, *Nature communications*, 2018, **9**, 1–11.

138 E. Kendrick, J. Kendrick, K. S. Knight, M. S. Islam and P. R. Slater, *Nature materials*, 2007, **6**, 871–875.

139 X. Kuang, M. A. Green, H. Niu, P. Zajdel, C. Dickinson, J. B. Claridge, L. Jantsky and M. J. Rosseinsky, *Nature materials*, 2008, **7**, 498–504.

140 M. Li, M. J. Pietrowski, R. A. De Souza, H. Zhang, I. M. Reaney, S. N. Cook, J. A. Kilner and D. C. Sinclair, *Nature materials*, 2014, **13**, 31–35.

141 L. Zhou and C. E. Boyd, *Aquaculture*, 2016, **450**, 187–193.

142 D. Thomas, M. Rey and P. Jackson, *Journal of Chromatography A*, 2002, **956**, 181–186.

143 J. Panchompoo and R. G. Compton, , 2012.

144 K. Waich, T. Mayr and I. Klimant, *Talanta*, 2008, **77**, 66–72.

145 A. LeDuy and R. Samson, *Biotechnology letters*, 1982, **4**, 303–306.

146 S. Z. Andersen, V. Čolić, S. Yang, J. A. Schwalbe, A. C. Nielander, J. M. McEnaney, K. Enemark-Rasmussen, J. G. Baker, A. R. Singh, B. A. Rohr, M. J. Statt, S. J. Blair, S. Mezzavilla, J. Kibsgaard, P. C. K. Vesborg, M. Cargnello, S. F. Bent, T. F. Jaramillo, I. E. L. Stephens, J. K. Nørskov and I. Chorkendorff, *Nature*, 2019.

147 Y. Zhao, R. Shi, X. Bian, C. Zhou, Y. Zhao, S. Zhang, F. Wu, G. I. Waterhouse, L.-Z. Wu, C.-H. Tung *et al.*, *Advanced Science*, 2019, **6**, 1802109.

148 D. Scheiner, *Water research*, 1976, **10**, 31–36.

149 X. Gao, Y. Wen, D. Qu, L. An, S. Luan, W. Jiang, X. Zong, X. Liu and Z. Sun, *ACS Sustainable Chemistry & Engineering*, 2018, **6**, 5342–5348.

150 Y. Zhao, R. Shi, X. Bian, C. Zhou, Y. Zhao, S. Zhang, F. Wu, G. I. N. Waterhouse, L.-Z. Wu, C.-H. Tung and T. Zhang, *Advanced Science*, 2019, **1802109**, 1802109.

151 G. Y. Duan, Y. Ren, Y. Tang, Y. Z. Sun, Y. M. Chen, P. Y. Wan and X. J. Yang, *ChemSusChem*, 2020, **13**, 88–96.

152 D. Midgley, *Ion-Selective Electrode Reviews*, Elsevier, 1982, vol. 3, pp. 43–104.

153 R. Y. Hodgetts, A. S. Kiryutin, P. Nichols, H.-L. Du, J. M. Bakker, D. R. Macfarlane and A. N. Simonov, *ACS Energy Letters*, 2020, **5**, 736–741.

154 B. H. R. Suryanto, C. S. M. Kang, D. Wang, C. Xiao, F. Zhou, L. M. Azofra, L. Cavallo, X. Zhang and D. R. Macfarlane, 2018.

155 H. Yu, R. Shi, Y. Zhao, T. Bian, Y. Zhao, C. Zhou, G. I. Waterhouse, L.-Z. Wu, C.-H. Tung and T. Zhang, *Advanced Materials*, 2017, **29**, 1605148.

156 S. Z. Andersen, V. Čolić, S. Yang, J. A. Schwalbe, A. C. Nielander, J. M. McEnaney, K. Enemark-Rasmussen, J. G. Baker, A. R. Singh, B. A. Rohr *et al.*, *Nature*, 2019, 1.

157 A. C. Nielander, J. M. McEnaney, J. A. Schwalbe, J. G. Baker, S. J. Blair, L. Wang, J. G. Pelton, S. Z. Andersen, K. Enemark-Rasmussen, V. Colic *et al.*, *Acs Catalysis*, 2019, **9**, 5797–5802.

158 Y. Song, C. Xu, H. Kuroki, Y. Liao and M. Tsunoda, *Journal of pharmaceutical and biomedical analysis*, 2018, **147**, 35–49.

159 Y. Song, D. Johnson, R. Peng, D. K. Hensley, P. V. Bonnesen, L. Liang, J. Huang, F. Yang, F. Zhang, R. Qiao *et al.*, *Science advances*, 2018, **4**, e1700336.

160 Y. Luo, G.-F. Chen, L. Ding, X. Chen, L.-X. Ding and H. Wang, *Joule*, 2019, **3**, 279–289.

161 J. Kong, A. Lim, C. Yoon, J. H. Jang, H. C. Ham, J. Han, S. Nam, D. Kim, Y.-E. Sung, J. Choi *et al.*, *ACS Sustainable Chemistry & Engineering*, 2017, **5**, 10986–10995.

162 M.-M. Shi, D. Bao, B.-R. Wulan, Y.-H. Li, Y.-F. Zhang, J.-M. Yan and Q. Jiang, *Advanced Materials*, 2017, **29**, 1606550.

163 S.-J. Li, D. Bao, M.-M. Shi, B.-R. Wulan, J.-M. Yan and Q. Jiang, *Advanced Materials*, 2017, **29**, 1700001.

164 D. Bao, Q. Zhang, F.-L. Meng, H.-X. Zhong, M.-M. Shi, Y. Zhang, J.-M. Yan, Q. Jiang and X.-B. Zhang, *Advanced Materials*, 2017, **29**, 1604799.

165 I. A. Amar, R. Lan, J. Humphreys and S. Tao, 2016.

166 R.-Q. Liu, Y.-H. Xie, J.-D. Wang, Z.-J. Li and B.-H. Wang, *Solid State Ionics*, 2006, **177**, 73–76.

167 D. S. Yun, J. H. Joo, J. H. Yu, H. C. Yoon, J.-N. Kim and C.-Y. Yoo, *Journal of Power Sources*, 2015, **284**, 245–251.

168 A. Shrivastava, V. B. Gupta *et al.*, *Chronicles of young scientists*, 2011, **2**, 21.

169 I. J. McPherson, T. Sudmeier, J. Fellowes and S. C. E. Tsang, *Dalton Transactions*, 2018.

170 L. F. Greenlee, J. N. Renner and S. L. Foster, *ACS Catalysis*, 2018, **8**, 7820–7827.

171 N. M. Tzollas, G. A. Zachariadis, A. N. Anthemidis and J. A. Stratis, *International Journal of Environmental and Analytical Chemistry*, 2010, **90**, 115–126.

172 A. Afkhami and R. Norooz-Asl, *Journal of the Brazilian Chemical Society*, 2008, **19**, 1546–1552.